9

Liquids and Their Interfaces

So far we have considered photons, electrons, phonons, and gas molecules. The transport processes of these energy carriers have many common characteristics and thus we have treated them in parallel. Transport in liquid is considerably more difficult to deal with. Compared to gases, liquids have molecules are closely packed and have short-range interactions, while compared to crystalline solids, liquids lack the periodicity of crystal structures. For these reasons, we cannot develop a parallel treatment for transport in liquids as we have done in previous chapters for other energy carriers. This chapter provides a brief description of transport processes in liquids and near the interfaces between liquids and their surrounding media, such as liquid–solid, liquid–liquid, and liquid–vapor interfaces.

We will start with a brief introduction to the methods used to deal with transport in bulk liquids. Historically, some of the earliest approaches were attempts to modify kinetic theory, particularly the Boltzmann equation, to include, for example, the finite size of liquid molecules and the potential interaction among molecules. The success of modified kinetic theories, however, is rather limited. Another line of development was pioneered by Einstein (1905) in his studies of the Brownian motion of particles in a liquid. Brownian motion was generalized by Langevin, and further developed by others in the linear response theory (Kubo et al., 1998). With the development of computational tools, the study of liquids has gradually shifted to computer simulations based on the linear response theory. In section 9.1, we will discuss the modification of the Boltzmann equation by Enskog, Einstein's Brownian motion theory, and the Langevin equation. The linear response theory will be discussed in chapter 10.

From the discussion on transport in bulk liquids, we will see that the transport processes involve not only kinetic energy exchange but also potential energy

exchange. For nanoscale liquid transport, the interfacial force and the interfacial potential may be very different from those in bulk liquids, and this can impact the transport processes. We thus spend a large fraction of this chapter discussing the interfacial forces and interface potential between liquids and their surroundings. Regretfully, since most studies of transport between liquids and their interfaces are based on computer simulations of small domains, general information on how interfacial forces and potentials impact the liquid transport processes remains scarce in the literature.

At the end of this chapter, we will discuss some size effects on the thermodynamic properties at liquid–vapor interfaces. These effects are obtained from thermodynamics and are, in general, well understood. With the increasing attention to nanotechnology, these effects have new applications. Computational simulations also provide some new insights into these phenomena.

9.1 Bulk Liquids and Their Transport Properties

9.1.1 Radial Distribution Function and van der Waals Equation of State

We often regard liquids as structureless. This is not exactly true! Surrounding every liquid molecule are other molecules and their positions cannot be completely random because (1) the finite size of the liquid molecule determines that there are only a few other molecules in its immediate surrounding, and (2) these few molecules are more or less stabilized by the interatomic potential. One measure of the structure of a liquid is the radial distribution function, $g(r)$, which is defined as

$$4\pi r^2 n g(r) dr = \begin{matrix}\text{the number of molecules with centers between} \\ r \text{ and } r+dr \text{ measured relative to a specific molecule}\end{matrix} \tag{9.1}$$

where $n(= N/V)$ is the average particle number density. Typical distributions of $g(r)$ for liquids, crystalline solids, and gases are shown in figure 9.1. The first peak in $g(r)$ for a liquid represents the coordination shell of nearest neighbors, the second peak represents the next nearest neighbors, and so on. The radial distribution function is a measure of the correlation of the atom under consideration with the surrounding atoms. Figure 9.1 indicates that after a few intermolecular distances the correlation between liquid atoms totally disappears. For example, in liquid argon, this occurs at around 20 Å (Boon and Yip, 1980). In contrast, the radial distribution function $g(r)$ is periodic for crystalline solids and is equal to one for ideal gases.

One use of the radial distribution function $g(r)$ is in the construction of the equation of states (Carey, 1999). From chapter 4, eqs. (4.14) and (4.15), we see that the equation of states can be constructed from the canonical partition function Z, which depends on the energy states of the system. For a liquid system, we can divide its energy into the sum of its kinetic and potential energy. It is easy to write down the kinetic energy expression for every molecule in the liquid system. The radial distribution can be used to construct an expression of the potential energy. For example, if the average potential energy between

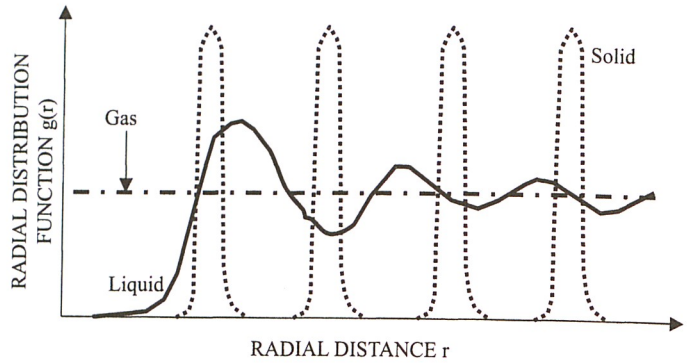

Figure 9.1 Typical behavior of the radial distribution function of liquids, crystalline solids (one-dimensional), and gases.

two molecules as a function of their separation r is $\phi(r)$, the total potential energy of an N-particle system is then

$$\Phi_N = \frac{N}{2}\int_0^\infty 4\pi r^2 \phi(r) n g(r) dr \tag{9.2}$$

The integral represents the potential interaction of one particle with the rest of the particles. $N/2$ includes all the particles in the system, where the factor $\frac{1}{2}$ accounts for the sharing of ϕ between two particles. One example of the potential distribution function is the Lennard–Jones potential between two molecules [see eq. (3.7)],

$$\phi(r) = 4\varepsilon\left[\left(\frac{\sigma}{r}\right)^{12} - \left(\frac{\sigma}{r}\right)^{6}\right] \tag{9.3}$$

where ε and σ are the Lennard–Jones potential parameters (table 3.1). We make a further assumption on the radial distribution function,

$$g(r) = \begin{cases} 0 & r < D \\ 1 & r \geq D \end{cases} \tag{9.4}$$

which means that there is no other molecule within a distance D surrounding the molecule, and outside D the other molecules are not correlated to the molecule. This is essentially a hard-sphere model for a molecule of diameter D. Under this model, eq. (9.2) can be expressed as

$$\Phi_N = -\frac{aN^2}{V} \tag{9.5}$$

where

$$a = -2\pi\int_D^\infty r^2 \phi(r) dr \tag{9.6}$$

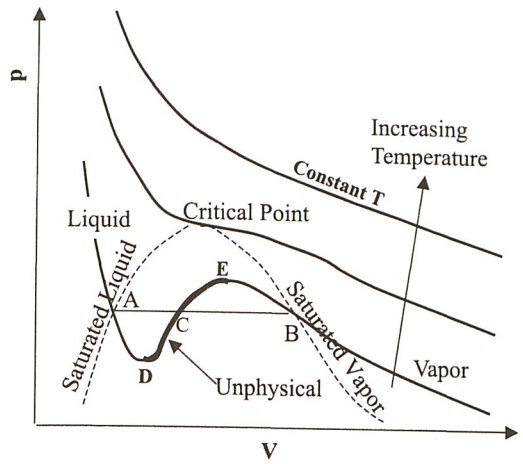

Figure 9.2 Isotherms predicted by the van der Waals equation. In region D–E, the pressure increases with increasing volume, which is unlikely to occur. Real systems avoid this region by a phase transition directly from A to B.

the negative sign ensuring that a is positive since the attractive part of the Lennard–Jones potential is negative. With eq. (9.5) for the potential energy, the canonical partition function can be derived for such a system (see, for example, Carey, 1999; Kittel and Kroemer, 1980). We will skip the details of the derivation and give the final canonical distribution function (the Helmholtz free energy) as

$$F(T, V, N) = -N\kappa_B T\left[\ln(V - BN) - \frac{3}{2}\ln\left(\frac{h^2}{2\pi m \kappa_B T}\right)\right] + \kappa_B T(N\ln N - N) - \frac{N^2 a}{V} \tag{9.7}$$

The above expression is an extension of eq. (4.28) for an ideal gas to a hard-sphere fluid. The extension includes two parts. One is the addition of the potential energy term we have just obtained. The other is to replace the volume in eq. (4.28) by $(V - BN)$, where B is the volume of an individual molecule. This correction accounts for the finite size of the molecules. From the Helmholtz free energy, the equation of states can be derived from $p = -(\partial F/\partial V)_{T,N}$ as

$$p = \frac{N\kappa_B T}{V - BN} - \frac{aN^2}{V^2} \tag{9.8}$$

The above equation is the celebrated van der Waals equation of states. Compared to the ideal gas equation of states, we see that BN accounts for the volume of the molecules and that the last term on the right-hand side represents the potential energy contribution to pressure.

The van der Waals equation of states is an idealized model that can describe both the vapor and the liquid phases (Goodstein, 1985). Figure 9.2 shows the isotherms of the equation of states on a p–V diagram. There exists a critical temperature below which the p–V curves have a local minimum (point D) and a local maximum (point E). Between the two extrema (DE), the pressure increases as the volume expands. This is an unphysical result. Real systems overcome this by a sudden change in volume to go

from point A to point B of the curve, which corresponds to the evaporation of liquid into vapor. Other familiar curves, such as the saturated liquid and saturated vapor lines, as well as the critical point, are also marked in the figure.

9.1.2 Kinetic Theories of Liquids

Given the great success of the Boltzmann kinetic theory for gases and, as we have seen, for electrons and phonons, it was natural to modify the Boltzmann equation for liquid transport (Enskog, 1922; Chapman and Cowling, 1953; Rice and Gray, 1965; Kohler, 1972). The Boltzmann equation applies only to dilute systems of particles, assuming that these particles occupy no volume and that their interactions are limited to the instant of their collision, which is much shorter than the time spent by the particles moving freely before and after the collision. Liquid molecules clearly violate these assumptions. The molecules in a liquid are closely packed. While the repulsion force between the molecules is strong and similar to that between gas molecules, the long-range attraction force can no longer be neglected because such a force is the very reason that holds the molecules together in the liquid.

In chapter 6, we explained that the Boltzmann equation is a one-particle distribution function approximation to the general Liouville equation. In this section, we continue to use f to denote this one-particle distribution function and $f^{(2)}$ to denote the two-particle distribution function. The one-particle distribution function is an average of the N-particle distribution function $f^{(N)}(t, \mathbf{r}_i, \mathbf{p}_i)$ in the Liouville equation over the rest of the $(N-1)$ particles, eq. (6.4), which is repeated here,

$$f(t, \mathbf{r}_1, \mathbf{p}_1) = \frac{N!}{(N-1)!} \int \cdots \int f^{(N)}(t, \mathbf{r}_i, \mathbf{p}_i) d\mathbf{r}_2 \ldots d\mathbf{r}_N d\mathbf{p}_2 \ldots d\mathbf{p}_N \tag{9.9}$$

We will drop the subscript 1 from here on. One can also define a two-particle distribution function

$$f^{(2)}(t, \mathbf{r}, \mathbf{p}, \mathbf{r}_2, \mathbf{p}_2) = \frac{N!}{(N-2)!} \int \cdots \int f^{(N)}(t, \mathbf{r}_i, \mathbf{p}_i) d\mathbf{r}_3 \ldots d\mathbf{r}_N d\mathbf{p}_3 \ldots d\mathbf{p}_N \tag{9.10}$$

This two-particle distribution function describes the joint probability distribution of finding particles 1 at $(\mathbf{r}, \mathbf{p})$ and particle 2 at $(\mathbf{r}_2, \mathbf{p}_2)$. Similarly, higher order distribution functions can also be defined. From the Liouville equation, a hierarchy of equations for each of the distribution functions can be derived (Liboff, 1998). The equation of the lower order will involve also the distribution of higher orders. For example, the governing equation for the first order distribution function in its general form, is

$$\frac{\partial f}{\partial t} + \mathbf{v} \bullet \nabla_{\mathbf{r}} f + \frac{\mathbf{F}}{m} \bullet \nabla_{\mathbf{v}} f = S(f, f^{(2)}) \tag{9.11}$$

The left-hand side comprises the familiar terms in the Boltzmann equation and the right-hand side is a generalized scattering term, which is a function of f and $f^{(2)}$. To close this equation, $f^{(2)}$ must be related to f. Similarly, governing equations for higher order terms must be truncated by introducing closure relations, as in turbulence modeling.

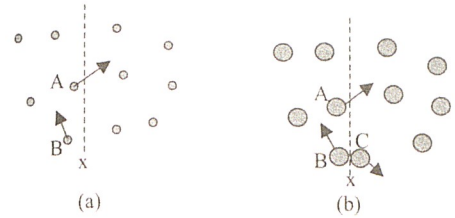

Figure 9.3 The difference between the Boltzmann kinetic formulation (a) and the Enskog formulation (b). In the Boltzmann formulation, heat flows across the interface at x only when the molecules (such as A) go across the interface. Molecules such as B do not contribute momentum and heat flux across x. In the Enskog model, even though B does not go across x, it collides with C and momentum and energy are transferred across the interface. This transfer occurs at a distance D and can be considered as due to the potential interaction between B and C.

The scattering integral in the Boltzmann equation, eq. (6.20), is based on the following assumption,

$$f^{(2)}(t, \mathbf{r}, \mathbf{p}, \mathbf{r}_2, \mathbf{p}_2) = f(t, \mathbf{r}, \mathbf{p}) f(t, \mathbf{r}_2, \mathbf{p}_2) \tag{9.12}$$

This expression means that no correlation exists between the position and the momentum of the colliding particles; this is called the molecular chaos assumption. For liquid, the long-range attraction force between molecules creates correlations among molecules and thus the above assumption is no longer valid. One approach to address this problem, taken by Rice and Allnatt (1961), is to derive a governing equation for $f^{(2)}$. The Rice–Allnatt equations and their solutions for even simple cases are very complex and will not be elaborated on here (see Rice and Gray, 1965). An earlier approach, taken by Enskog (Enskog, 1922; Chapman and Cowling, 1953, Velarde, 1974), is more intuitive and will be briefly discussed here. The Enskog model assumes that the liquid molecules are hard spheres of diameter D, and neglects long-range attracting forces. However, such long-range interactions are implicitly included in the Enskog model. Referring to figure 9.3, in the Boltzmann equation model, momentum and energy transfer across an imaginary plane x occurs only when a molecule, such as A, goes across the plane. In the Enskog model, however, momentum and energy transfer across plane x occurs in a collision between molecules B and C, even if molecule B does not go across this plane. Because of the finite diameter of the molecules, this latter process occurs when the two molecules are within a distance D in the Enskog hard sphere model. Enskog assumed that the two-particle distribution is related to the one-particle distribution function through the radial distribution function g:

$$f^{(2)}(t, \mathbf{r}, \mathbf{p}, \mathbf{r}_2, \mathbf{p}_2) = f(t, \mathbf{r}, \mathbf{p}) f(t, \mathbf{r}_2, \mathbf{p}_2) g(|\mathbf{R}_{12}|) \tag{9.13}$$

where $\mathbf{R}_{12} = \mathbf{r}_1 - \mathbf{r}_2$. In addition, due to the finite size of the particles, they do not occupy the same location at the moment of collision but are separated by a distance D. The Enskog equation may be written as (Chapman and Cowling, 1953; Kohler, 1972; Ferziger and Kaper, 1972; Velarde, 1974)

$$\frac{\partial f}{\partial t} + \mathbf{v} \cdot \nabla_{\mathbf{r}} f + \frac{\mathbf{F}}{m} \cdot \nabla_{\mathbf{v}} f = S \tag{9.14}$$

with the following expression for the scattering term,

$$S = \iint D^2\hat{\boldsymbol{\Omega}} \cdot (\mathbf{v}_2 - \mathbf{v}) d\Omega \, d^3\mathbf{p}_2 \times \left[g\left(\left|\mathbf{r} + \frac{1}{2}D\hat{\boldsymbol{\Omega}}\right|\right) f(t, \mathbf{r}, \mathbf{p}') f(t, \mathbf{r} + D\hat{\boldsymbol{\Omega}}, \mathbf{p}_2') - g\left(\left|\mathbf{r} - \frac{1}{2}D\hat{\boldsymbol{\Omega}}\right|\right) f(t, \mathbf{r}, \mathbf{p}) f(t, \mathbf{r} - D\hat{\boldsymbol{\Omega}}, \mathbf{p}_2) \right] \tag{9.15}$$

where the superscript $'$ represents properties after collision, $\hat{\boldsymbol{\Omega}}$ is the unit vector connecting the centers of the two colliding spherical molecules and the integration of $d\Omega$ means over the entire solid angle formed between the two molecules. The first term inside the square brackets represents the in coming scattering into $(\mathbf{r}, \mathbf{p})$ and the second term is the out going scattering. From momentum conservation, $\mathbf{p}'$ and $\mathbf{p}_2'$ are related to $\mathbf{p}$ and $\mathbf{p}_2$ by

$$\mathbf{p}' = \mathbf{p} + \hat{\boldsymbol{\Omega}}[(\mathbf{p}_2 - \mathbf{p}) \bullet \hat{\boldsymbol{\Omega}}] \quad \mathbf{p}_2' = \mathbf{p}_2 - \hat{\boldsymbol{\Omega}}[(\mathbf{p}_2 - \mathbf{p}) \bullet \hat{\boldsymbol{\Omega}}] \tag{9.16}$$

Solution of the Enskog equation leads to the following expressions for the viscosity and thermal conductivity of liquids (Kohler, 1972; Ferziger and Kaper, 1972; Velarde, 1974):

$$\mu_E = \frac{\mu_0}{g(D)}\left[1 + \frac{4}{15}\pi n D^3 g(D)\right]^2 + \frac{3}{5}\Pi \tag{9.17}$$

$$k_E = \frac{k_0}{g(D)}\left[1 + \frac{2}{5}\pi n D^3 g(D)\right]^2 + \frac{3\kappa_B}{2m}\Pi \tag{9.18}$$

$$\mu_0 = \frac{5}{16}\frac{\sqrt{\pi m \kappa_B T}}{D^2 \pi} \tag{9.19}$$

$$k_0 = \frac{25}{32}\frac{\sqrt{\pi m \kappa_B T}}{D^2 \pi}\frac{3\kappa_B}{2m} \tag{9.20}$$

$$\Pi = \frac{4}{9}\sqrt{\pi m \kappa_B T} n^2 D^4 g(D) \tag{9.21}$$

$$g = \frac{(1 - 11nb/9)}{1 - 2nb} \tag{9.22}$$

$$b = \frac{2}{3}\pi D^3 \tag{9.23}$$

where the subscript E represents Enskog results, and k_0 and μ_0 are the kinetic theory results for dilute gases [eq. (6.68a)]. These expressions can be written in normalized form as

$$\frac{\mu_E}{\mu_0} = bn\left(\frac{1}{y} + 0.8 + 0.76y\right) \tag{9.24}$$

$$\frac{k_E}{k_0} = bn\left(\frac{1}{y} + 1.2 + 0.76y\right) \tag{9.25}$$

where $y = nbg(D)$. In using the above expressions to calculate the transport coefficient, the key is to calculate an effective diameter D for the gas molecules. This can be done, for example, on the basis of experimental data on dilute gases and from eq. (9.19) or (9.20). Once the diameter is obtained, μ_E and k_E can be calculated as a function of the mass density (or the molecular number density n) (Sengers, 1965).

Both the viscosity and the thermal conductivity expressions can be interpreted as the result of a kinetic contribution, a collisional contribution, which is equivalent to potential contribution, and a cross-coupling term between the kinetic and collisional processes. Taking the thermal conductivity as an example, these two contributions can be expressed as

$$\frac{k_E}{k_0 nb} = \frac{1}{y} + 1.2 + 0.76y = \text{kinetic} + \text{cross} + \text{collisional} \tag{9.26}$$

which shows that the importance of the kinetic contribution decreases as the density increases, whereas the collisional contribution increases with density. Figure 9.4 compares the results of molecular dynamics simulation with the results from the Enskog equation for each of the three terms (Alder et al., 1970), showing good agreement for $V \geq 5V_0$ or $n \leq 0.2n_0$, where V_0 and n_0 are the volume and number density when the molecules are close packed. At higher densities, significant deviations occur. Near solidification, for example, the Enskog theory underestimates the shear viscosity by a factor of two.

Despite the work of Enskog and many others, the success of the kinetic theory for liquids, is limited. With the advance of computational power, direct simulation of liquid molecules, that is, molecular dynamics, and the analysis of the simulation using linear response theory, have largely replaced the kinetic theory approach for the study of liquid transport properties. In chapter 10, we will discuss in more detail some molecular dynamics simulation techniques and the linear response theory. In the following, we will discuss Brownian motion. Einstein (1905) pioneered an entirely different approach from that of the Boltzmann equation to study Brownian motion in liquids, and this eventually led to the development of the linear response theory.

9.1.3 Brownian Motion and the Langevin Equation

Einstein is best known for his relativity theory. Few people are familiar with his work on Brownian motion, which was a key step in the development of the atomic theory of matter. Research on Brownian motion was carried out by Einstein (1905, 1906a, 1906b, 1956) for his doctoral dissertation when he was an engineer in a patent office in Bern,

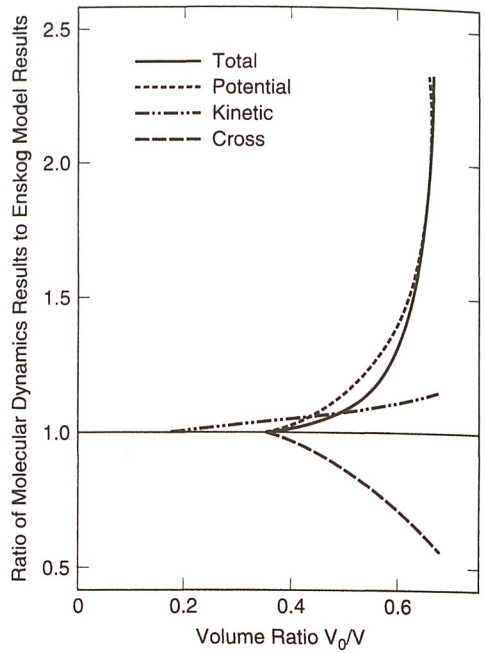

Figure 9.4 Shear viscosity of a hard-sphere fluid, calculated from molecular dynamics, relative to its Enskog values for contributions from the kinetic, the potential, and cross terms, where $V_0 = ND^3/\sqrt{2}$ is the volume at close packing (after Alder et al., 1970).

Switzerland. In fact, when he wrote his first paper on the Brownian motion in 1905, he was unaware that Brownian motion had been observed by botanist Brown in 1827. His motivation was to determine the size of molecules. Prior to his work, the well-established Boltzmann kinetic theory was applicable only to gases. He intended to develop a kinetic theory for liquids and, from the theory, to determine the size of the molecules.

Einstein considered the mass transfer of dilute solutes in a solvent. He first proved, from statistical thermodynamics, that the solute generates an additional pressure, called the osmotic pressure, that can be expressed as

$$p = \frac{1}{V} N\kappa_B T = n\kappa_B T \tag{9.27}$$

where N is the number of solute particles in the total solution volume V and $n = N/V$ is the solute concentration per unit volume. This expression is similar to the ideal gas law and is valid only when the solute is dilute, similar to the condition of an ideal gas. This osmotic pressure can be measured by an osmometer, which employs a semi-permeable membrane that permits the crossing of only the solvent, not the solute (Hiemenz, 1986). Einstein considered next the mass diffusion of solute particles under a concentration gradient of the particles (Einstein, 1908). The osmotic pressure drives the diffusion of the solute particles. When the solute particles traverse the solvent, they experience a drag that can be modeled by the well-established Stokes law in continuum fluid mechanics,

$$\mathbf{F}_D = 3\pi\mu D\mathbf{u} \tag{9.28}$$

where μ is the dynamic viscosity, D the particle diameter, and $\mathbf{u}$ the particle velocity. At steady state, the osmotic pressure force is balanced by the frictional force on the particles, leading to a steady drift velocity that is determined by the following balance equation,

$$A_c[p(x) - p(x+dx)] - dN(3\pi D\mu)u_x = 0 \tag{9.29}$$

for particles drifting in the x-direction, where dN is the number of solute particles in the volume $dV = A_c dx$. Substituting eqs. (9.27) into (9.29) leads to

$$nu_x = -\frac{\kappa_B T}{3\pi D\mu}\frac{dn}{dx} \tag{9.30}$$

The left-hand side is the volume flux of the solute particles. Thus the above equation is just Fick's law of diffusion,

$$J_x = -a\frac{dn}{dx} \tag{9.31}$$

where the diffusivity $a[\mathrm{m^2\,s^{-1}}]$ is related to the viscosity by

$$a = \frac{\kappa_B T}{3\pi D\mu} \tag{9.32}$$

Equation (9.32) is the celebrated Einstein relation. If both a and μ are known, the diameter of the Brownian particle can be estimated, as was Einstein's original intent. This expression is similar to eq. (6.86), which is also called the Einstein relation. Equation (6.86) is an electron analogy to what Einstein actually derived for Brownian particles, except that in eq. (6.86) the electron mobility is a measure of how mobile the charge is; that is, the higher the mobility, the larger the diffusivity and conductivity of electrons. By contrast, the viscosity in eq. (9.32) is a measure of the resistance to the particle flow and thus is in the denominator rather than the numerator.* The Einstein relation shows an intrinsic relationship between transport properties (diffusivity) and the internal friction (viscosity), and is one example of the general fluctuation–dissipation theorem that we will discuss in the next chapter.

Equation (9.32) reflects Einstein's motivation of determining the diameter of the solute molecules, which are assumed to be much larger than those of the solvent, from the diffusivity of the solute in the solvent. Another question is how to determine the solute diffusivity. Einstein further showed, by solving the mass balance equation, that the mean displacement of the solute particles, for transport along the x-direction only, is

$$\langle \Delta x \rangle = \langle (x(t) - x(0))^2 \rangle^{1/2} = \sqrt{2at} \tag{9.33}$$

while for motion in a three-dimensional space the mean displacement is given by

$$\langle \Delta \mathbf{r} \rangle = \langle (|\mathbf{r}(t) - \mathbf{r}(0)|)^2 \rangle^{1/2} = \sqrt{6at} \tag{9.34}$$

*We have used μ to present both the mobility of electrons in eq. (6.86) and the viscosity of a fluid, as is customary in electronics and fluid mechanics, despite the opposite meaning of these two quantities.

where $x(t)$ and $r(t)$ are the instantaneous position of the particle. Thus, from measuring the mean displacement of the solute, the diffusivity can be determined.

In addition to the above approach, Einstein established another method to determine the diameter of solute particles. He proposed to measure the viscosity of the solvent and of the solution, μ_0, and μ, respectively, and derived, again assuming dilute solute particles, the following relationship between the two viscosities,

$$\frac{\mu}{\mu_0} = 1 + 2.5\varphi = 1 + 2.5n\frac{1}{6}\pi D^3 \tag{9.35}$$

where φ is the volumetric concentration of the solute particles. We will not repeat Einstein's derivation but instead refer the reader to his original work (1906a; 1956). This result again applies only to dilute solutes. Many studies have been done to extend his results to higher volumetric concentrations (Hiemenz, 1986). These works should be a good starting point to examine recent claims on the novel properties of nanoparticle-seeded fluids, also referred to as nanofluids (Choi et al., 2001).

The Einstein relation can also be derived from the stochastic approach developed by Langevin to treat Brownian motion of particles much larger than those of the surrounding medium. The key idea of the Langevin equation is to assume that the motion of a Brownian particle is subject to a frictional force that is linearly proportional to its velocity, as in the Stokes law [eq. (9.28)], and a random driving force, $\mathbf{R}(t)$, imparted by the random motion of the molecules in the bath. The requirement that the Brownian particle is much larger in size than the molecules in the bath implies that the collision time of the bath molecules with the Brownian particle is much shorter than the relaxation time of the Brownian particle from its initial velocity, and hence there is no time correlation between the Brownian particle velocity and the molecular velocity. In the absence of an external force, the Langevin equation that governs the instantaneous velocity of the Brownian particle can be written as

$$m\frac{d\mathbf{u}}{dt} = -m\eta\mathbf{u} + \mathbf{R}(t) \tag{9.36}$$

where η is the friction coefficient for Brownian particles in a fluid. The Stokes law gives $\eta = 3\pi D\mu/m$. The random driving force $\mathbf{R}(t)$ has the following characteristics:

$$\langle \mathbf{R}(t) \rangle = 0 \tag{9.37}$$

$$\langle \mathbf{R}(t) \cdot \mathbf{u}(t) \rangle = 0 \tag{9.38}$$

$$\langle \mathbf{R}(t+s) \cdot \mathbf{R}(s) \rangle = 2\pi R_0 \delta(t) \tag{9.39}$$

where the bracket $\langle\rangle$ represents the ensemble average, a concept we discussed in chapter 4. Equation (9.37) indicates that the random driving force averages to zero because it acts in all directions. Equation (9.38) states that the random driving force is not correlated to the velocity of the Brownian particle. This can be justified if the Brownian particle size is large and its velocity relaxation time is much longer than the characteristic fluctuation time of the random driving force. Equation (9.39) implies that the autocorrelation of the random driving force is infinitely short.

Now, we show how to derive the Einstein relation from the Langevin equation. Taking the inner product of both sides of eq. (9.36) with $\mathbf{r}(t)$, the instantaneous position of the Brownian particle, and utilizing the relation

$$\mathbf{r} \cdot \frac{d\mathbf{u}}{dt} = \mathbf{r} \cdot \frac{d^2\mathbf{r}}{dt^2} = \frac{1}{2}\frac{d^2|\mathbf{r}^2|}{dt^2} - |\mathbf{u}|^2 \tag{9.40}$$

we obtain

$$\frac{1}{2}m\frac{d^2|\mathbf{r}^2|}{dt^2} + \frac{1}{2}m\eta\frac{d|\mathbf{r}^2|}{dt} = m|\mathbf{u}^2| + \mathbf{r}(t) \cdot \mathbf{R}(t) \tag{9.41}$$

By ensemble averaging, the last term on the right-hand side of the above equation drops out because there is no correlation between the particle instantaneous position and the random driving force. Applying the equipartition theorem,

$$\langle |\mathbf{u}(t)|^2 \rangle = \frac{3\kappa_B T}{m} \tag{9.42}$$

we obtain from eq. (9.41)

$$\frac{1}{2}m\frac{d^2\langle|\mathbf{r}^2|\rangle}{dt^2} + \frac{1}{2}m\eta\frac{d\langle|\mathbf{r}^2|\rangle}{dt} = 3\kappa_B T \tag{9.43}$$

The initial conditions for the above differential equation are

$$\langle |\mathbf{r}(0)|^2 \rangle = 0 \tag{9.44}$$

$$\frac{d}{dt}\langle |\mathbf{r}(0)|^2 \rangle = 2\langle \mathbf{r}(0) \cdot \mathbf{u}(0) \rangle = 0 \tag{9.45}$$

Equation (9.43) can be readily solved with the above initial conditions, leading to

$$\langle |\mathbf{r}\,(t)|^2 \rangle = \left(\frac{6\kappa_B T}{\eta m}\right)\left(t - \frac{1}{\eta} + \frac{1}{\eta}e^{-\eta t}\right) \tag{9.46}$$

At large times such that $\eta t \gg 1$, eq. (9.46) becomes

$$\langle |\mathbf{r}(t)|^2 \rangle = \left(\frac{6\kappa_B T}{\eta m}\right)t \tag{9.47}$$

Combining eq. (9.47) with eq. (9.34) leads to the Einstein relation

$$a = \frac{\kappa_B T}{\eta m} \tag{9.48}$$

This is identical to eq. (9.32), if we substitute $\eta = 3\pi D\mu/m$.

From the Langevin equation, one can also derive another way to calculate the friction coefficient. We start by integrating eq. (9.36) directly for a solution of the velocity. Strictly speaking, because the driving force is random, direct integration of eq. (9.36) is problematic from a mathematical point of view. This difficulty can be overcome by spectral analysis of the equation. Here, however, we will put aside the mathematical

rigor and integrate eq. (9.36) directly as if $\mathbf{R}(t)$ were a continuous function. The end results are the same as those from a rigorous mathematical treatment. Integration of eq. (9.36) leads to

$$m\mathbf{u}(t) = m\mathbf{u}(0)e^{-\eta t} + e^{-\eta t}\int_0^t e^{\eta s}\mathbf{R}(s)ds \tag{9.49}$$

Taking the dot product of eq. (9.49) with $\mathbf{u}(0)$, we have

$$m\mathbf{u}(t)\cdot\mathbf{u}(0) = m\mathbf{u}(0)\cdot\mathbf{u}(0)e^{-\eta t} + e^{-\eta t}\int_0^t e^{\eta s}\mathbf{R}(s)\cdot\mathbf{u}(0)ds \tag{9.50}$$

Ensemble-averaging the above equation yields

$$\langle\mathbf{u}(t)\cdot\mathbf{u}(0)\rangle = \langle\mathbf{u}(0)\cdot\mathbf{u}(0)\rangle e^{-\eta t} = \frac{3\kappa_B T}{m}e^{-\eta t} \tag{9.51}$$

The ensemble average of the product of the same time-varying function at two different times $\langle A(t)A(t')\rangle$ is called the autocorrelation function, which again will be defined more carefully in chapter 10. In eq. (9.51), the left-hand side is the velocity autocorrelation function. By integrating both sides of the above equation from $t = 0$ to $t \to \infty$, the following expression for the friction coefficient can be obtained,

$$\int_0^\infty \langle\mathbf{u}(t)\cdot\mathbf{u}(0)\rangle dt = \frac{3\kappa_B T}{\eta m} = 3a \tag{9.52}$$

Equation (9.52) shows that the friction coefficient and thus the diffusivity can be calculated from the velocity autocorrelation function. This approach of calculating the transport properties from the auto correlation functions has gained popularity with increasing computational power, because the history of individual particles can be monitored through molecular dynamics simulation, as we will see in the next chapter. Modern treatments of liquids rely heavily on computational simulations (Alder and Wainwright, 1967; Boon and Yip, 1980; Hansen and McDonald, 1986). For example, the molecular dynamic calculations of Alder and Wainwright (1967) showed that the velocity autocorrelation decays much slowly than the exponential function suggested by eq. (9.46) and by the Enskog theory. Figure 9.4 shows another example where molecular dynamics is used to examine the validity of the Enskog equation. We will leave more discussion on the molecular dynamics simulations to the next chapter.

9.2 Forces and Potentials between Particles and Surfaces

The discussion in the previous section shows that for transport in liquids the intermolecular potential plays a direct role in energy and momentum exchange. For liquid transport in nanostructures, we naturally expect that the forces and potentials between

the liquid molecules and their surroundings may become important. In our previous consideration of boundary effects on the transport of dilute particles, based on the Boltzmann equation or on wave propagation, the boundary impacts the transport only at the point of particle trajectory or wavefunction overlapping with the boundary because potential energy does not directly enter into the transport picture. On the other hand, because dilute particles have relatively long mean free paths, a collision that occurs at the boundary can affect the distribution quite far from the interface. Liquid molecules, however, have short mean free paths, suggesting that boundary effects will most likely be limited to the region where the interfacial potential changes significantly from that in the bulk fluid. Despite this relatively straightforward argument, however, few studies exist on how the interface potential impacts the transport properties. Most investigations have so far been based on nonequilibrium molecular dynamics methods (Koplik and Banavar, 1995; Thompson and Troian, 1997). On the other hand, there exists quite a large literature on the forces and potentials between liquids and their interfaces, arising from studies on surface tension, colloids, and complex fluids. Understanding such potentials and forces is an important step in appreciating the interfacial transport processes and incorporating them into either modeling or direct molecular dynamic simulations. In this section, we will briefly summarize the interfacial interactions. We will start from the intermolecular potentials to build expressions for interactions among surfaces, expressed in terms of forces or interaction potentials. These surface interactions include van der Waals interactions, which are typically attractive, and electrostatic interactions that are typically repulsive, and other forces arising from the structure of the molecules and the interfaces. We will talk about forces and potentials interchangeably, with the understanding that force is related to the potential through

$$\mathbf{F} = -\nabla\Phi \tag{9.53}$$

9.2.1 Intermolecular Potentials

Fundamentally, all the interatomic and intermolecular potentials are due to electrostatic interactions. In chapter 3, we discussed bonding forces in crystals, such as van der Waals bonding, ionic bonding, covalent bonding, and metallic bonding. In solids, the force interactions are mainly due to electrostatic interactions among atoms. In liquids, a greater variety of force interactions exists because liquids are made of molecules and have more degrees of freedom. Figure 9.5 summarizes common types of interactions between atoms, ions and molecules in vacuum and the corresponding interaction potential Φ (relative to the energy of the system in vacuum when the two parts are far apart) (Israelachvili, 1992). The basic building block for all these potentials is the Coulomb potential between two single charged particles, from which one can derive other types of interaction potential based on the charge configurations in atoms and molecules.

Example 9.1 *Charge–dipole interaction*

A dipole consists of two oppositely charged particles separated by a distance d. Derive an expression for the potential between a charge and a fixed dipole in vacuum, that is, the third line in figure 9.5.

Type of Interactions		Interaction Potential ϕ
Covalent	 (H_2O)	strong, complicated, short range
Charge-Charge	 ($NaCl$)	$\frac{q_1 q_2}{4\pi\varepsilon_o r}$ Coulomb Potential
Charge-Dipole	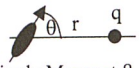 Dipole Moment β	$-\frac{\beta q \cos\theta}{4\pi\varepsilon_o r^2}$ (Fixed Dipole) $-\frac{(\beta q)^2}{6(4\pi\varepsilon_o)^2 r^4 \kappa_B T}$ (Free Rotating)
Dipole-Dipole	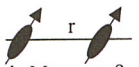 Dipole Moments β_1 and β_2	$-\frac{(\beta_1\beta_2)^2}{3(4\pi\varepsilon_o)^2 r^6 \kappa_B T}$ (Free Rotating)
Charge-Nonpolar	 Polarizability α	$-\frac{q^2\alpha}{2(4\pi\varepsilon_o)^2 r^4}$
Polar-Nonpolar	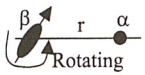 Rotating	$-\frac{\beta^2\alpha}{(4\pi\varepsilon_o)^2 r^6}$ Debye Energy
Two Non-Polar Molecules		$-\frac{3}{4}\frac{h\nu\alpha^2}{(4\pi\varepsilon_o)^2 r^6}$ London Dispersion Energy
Hydrogen Bond	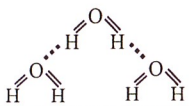	complicated, short range, roughly ~ $-1/r^2$

Figure 9.5 Common types of interaction between atoms, ions, and molecules in vacuum (after Israelachvili, 1992).

Solution: Consider a charge q placed in the field of the dipole, as shown in figure E9.1. The potential energy between the charge and the dipole can be thought of as the superposition of the potential energy of charge q interacting with Q and $-Q$, respectively,

$$\phi = -\frac{Qq}{4\pi\varepsilon_0}\left[\frac{1}{AB} - \frac{1}{AC}\right] \tag{E9.1.1}$$

where

$$AB = \left[\left(r - \frac{d}{2}\cos\theta\right)^2 + \left(\frac{d}{2}\sin\theta\right)^2\right]^{1/2} \tag{E9.1.2}$$

$$AC = \left[\left(r + \frac{d}{2}\cos\theta\right)^2 + \left(\frac{d}{2}\sin\theta\right)^2\right]^{1/2} \tag{E9.1.3}$$

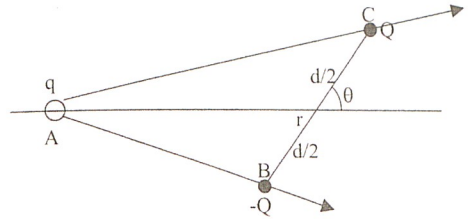

Figure E9.1 Figure for example 9.1.

In writing eq. (E9.1.1), we did not include the potential energy of the positive and negative charge of the dipole itself, which is included in the dipole self-energy. Substituting eqs. (E9.1.1) and (E9.1.2) into eq. (E9.1.3) and making use of the approximation that $r \gg d$, we obtain

$$\phi(r,\theta) = -\frac{q\beta\cos\theta}{4\pi\varepsilon_0 r^2} \tag{E9.1.4}$$

where $\beta = Qd$ is the dipole moment.

Comment. If the dipole is freely rotating, we can obtain the angle-averaged potential based on the Boltzmann factor

$$e^{-\bar{\phi}(r)/kT} = \frac{1}{4\pi}\int e^{-\phi(r,\theta)/\kappa_B T} d\Omega \tag{E9.1.5}$$

where the integration is over the entire solid angle. Using Taylor expansion for the exponential factor, one can show (Israelachvili, 1992)

$$\bar{\phi}(r) \approx -\frac{q^2\beta^2}{6(4\pi\varepsilon_0)^2\kappa_B T r^4} \tag{E9.1.6}$$

9.2.2 Van der Waals Potential and Force between Surfaces

On the basis of the elementary potential interactions discussed in the previous section, the force interaction between particles and surfaces can be obtained by summing up the interactions between the atoms or molecules involved. Such a summation often leads to qualitatively different behavior compared to the elementary forces between charge and atoms given in figure 9.5.

Starting from the attractive van der Waals potential between two atoms, $\phi(r) = -C/r^6$, one may sum the interaction energies of all the atoms in one body that interact with all the atoms in the other to obtain the interaction potential between the two bodies for a variety of geometries that are listed in figure 9.6 (Israelachvili, 1992). In this figure, A is called, the Hamaker constant (Hamaker, 1937)

$$A = \pi^2 C n_1 n_2 \tag{9.54}$$

where n_1 and n_2 are the number densities of molecules of the two interacting media. A typical values of C is 10^{-77} J m^6 and $n \approx 3 \times 10^{28}$ m^{-3}, leading to $A \approx 10^{-19}$ J. For example, for water, $A = 1.5 \times 10^{-19}$ J and for CCl_4, $A = 0.5 \times 10^{-19}$ J.

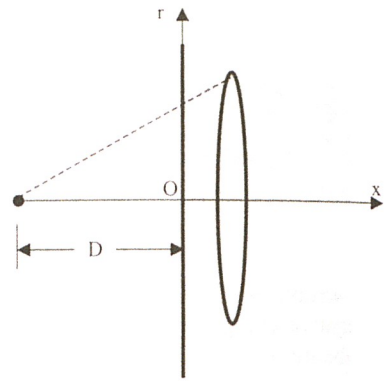

Figure E9.2 Figure for example 9.2.

Example 9.2 Derive an expression for the van der Waals potential between one atom and a surface.

Solution: We take a coordinate system as shown in figure E9.2. The atom is at equal distance from all parts of a differential ring inside the surface and thus all the atoms on the ring experience the same potential. The van der Waals attracting potential between the atom and this differential volume of $2\pi r^2 dr dx$ is

$$d\Phi = -\frac{C}{\left(\sqrt{(D+x)^2+r^2}\right)^6} n 2\pi r\, dr\, dx \qquad \text{(E9.2.1)}$$

Integrating the above expression for x from D to ∞ and for r from 0 to ∞, we obtain

$$\Phi = -\frac{\pi C n}{6D^3} \qquad \text{(E9.2.2)}$$

which is identical to the formula in figure 9.6(b).

In example 9.2, and similarly for all cases in figure 9.6, we neglected the influence of the atoms inside the same solid and assumed that the medium between the two surfaces is vacuum. This treatment always leads to a positive Hamaker constant and thus an attractive potential between the two bodies. An alternative approach is the Lifshitz (1956) theory, which neglects the atomic structure and treats the objects as continuous media. The final expressions are similar to those listed in figure 9.6 but the Hamaker constant between surfaces 1 and 2, separated by a medium 3, can be expressed in terms of the dielectric constants of the media. If all three media are dielectrics and the electronic excitation frequencies are the same (ν_e), the Hamaker constant from the Lifshitz theory can be approximated as

$$A \approx \frac{3}{4}\kappa_B T \left(\frac{\varepsilon_{r1}-\varepsilon_{r3}}{\varepsilon_{r1}+\varepsilon_{r3}}\right)\left(\frac{\varepsilon_{r2}-\varepsilon_{r3}}{\varepsilon_{r2}+\varepsilon_{r3}}\right) + \frac{3h\nu_e}{8\sqrt{2}} \frac{(n_{r1}^2-n_{r3}^2)(n_{r2}^2-n_{r3}^2)}{\sqrt{(n_{r1}^2+n_{r3}^2)(n_{r2}^2+n_{r3}^2)}\left[\sqrt{n_{r1}^2+n_{r3}^2}+\sqrt{n_{r2}^2+n_{r3}^2}\right]} \qquad (9.55)$$

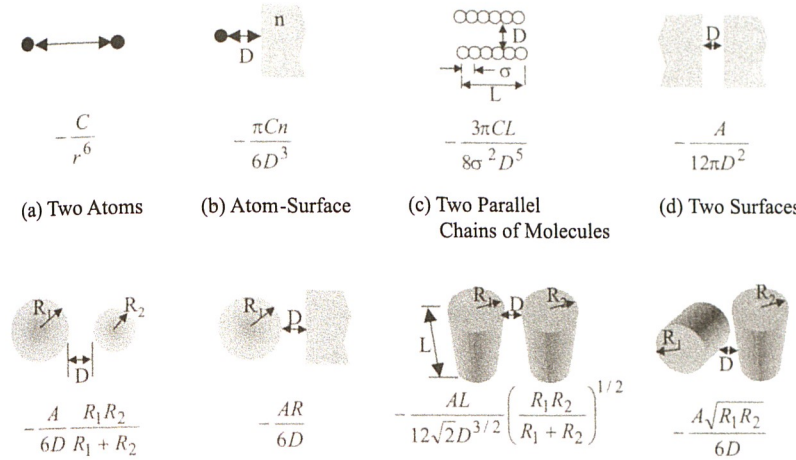

Figure 9.6 Van der Waals interaction free energies between two bodies. The Hamaker constant $A = \pi^2 C n_1 n_2$, where n_1 and n_2 are the atom number densities in the two media and C is the coefficient in the atom–atom pair potential (after Israelachvili, 1992).

where ε_r is the static dielectric constant (at zero frequency), n_r is the refractive index in the visible frequency range, and the number in the subscript represents the medium. The purpose for showing the above formula is to demonstrate the possibility of negative Hamaker constant values and thus a repulsive van der Waals force between two macroscopic objects, separated by a third medium, depending on the relative magnitudes of the dielectric constants of the media involved. Such negative Hamaker constant values have indeed been observed, for example, between fused quartz and air, separated by a water layer, and between CaF_2 and helium vapor, separated by liquid helium.

The van der Waals force between surfaces is also called the London force or dispersion force. This potential is universal among all surfaces because it arises from the induced dipoles among atoms.

9.2.3 Electric Double Layer Potential and Force at Interfaces

Surfaces immersed in liquids are usually charged because of the ionization or dissociation of surface groups or the adsorption of ions from the solution onto a previously uncharged surface [figure 9.7(a)]. The charges accumulated at the surface are balanced by an equal but oppositely charged region of counterions. Some of these counterions are also bounded to the surface, forming a so-called Stern or Helmholtz layer, which is usually very thin (a few angstroms). The remaining counterions distribute near the surfaces but are free to move, forming a diffuse electric double layer. This electric double layer is of fundamental importance for a wide range of technologies such as batteries, fuel cells, colloids, and in biochemistry and biotechnology.

We first determine the magnitude of the potential developed on the solid–liquid interface. This potential can be easily measured, using the solid as an electrode. Under the

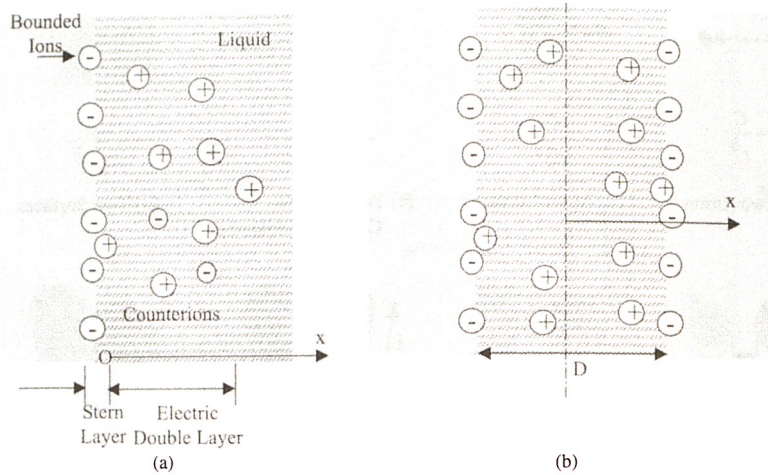

Figure 9.7 (a) Electrical double layer near the interfacial region. The charge on the surface can be due to dissociation or ionization of the surface materials or adsorption from the liquid. The charges in the liquid can be of multiple species. (b) A repulsive potential develops between two closely spaced surfaces when the charges in the liquids are of only one type, due, for example, to ionization or dissociation from the surface.

condition of local equilibrium, the ion density on the solid surface obeys the Boltzmann distribution

$$c_s = c_{zp} e^{-Ze\psi_s/\kappa_B T} \tag{9.56}$$

where Z is the number of charges per ions and e is the unit charge ($-e$ for an electron), ψ_s is the electrostatic potential of the solid surface, and c_{zp} is the ion density at zero surface electrostatic potential. Equation (9.55) can be written as

$$\psi_s = -\frac{\kappa_B T}{e} \ln\left(\frac{c_s}{c_{zp}}\right) = \frac{\kappa_B T}{e} \ln\left(\frac{n}{n_{zp}}\right) \tag{9.57}$$

where n and n_{zp} are the counterion densities in the solution corresponding to c_s and c_{zp} which are much easier to measure than the charge densities on the solid side. Equation (9.57) is called the Nernst equation. This is very similar to the Seebeck coefficient expression we derived in example 6.1.

As an example, consider a saturated solution of AgI in pure water with a solid AgI electrode. The saturated solution has equal amounts of 8.7×10^{-9} moles per liter (mol L^{-1}) of Ag^+ and I^- ions at 25°C. It is found experimentally that the AgI electrode is negatively charged in this situation, meaning that more I^- ions are adsorbed on the surface. At zero potential, the Ag^+ concentration is 3×10^{-6} mol L^{-1}. Using eq. (9.57), the Nernst potential is $\psi_s = -150$ mV.

To find the ion distribution near the surface, we need to solve the following equation governing the distribution of electrostatic potential ψ that can be derived from eq. (5.13),

$$-\varepsilon_0 \varepsilon_r \nabla^2 \psi = \rho_n \tag{9.58}$$

where ε_r is the dielectric constant and ρ_n is the net charge number density. The charge distribution in the solution is also given by the Boltzmann distribution, leading to the Poisson–Boltzmann equation

$$-\varepsilon_0 \varepsilon_r \nabla^2 \psi = \sum_i Z_i e n_{0i} \exp\left(-\frac{Z_i e \psi}{\kappa_B T}\right) \tag{9.59}$$

where n_{0i} is the ion concentration far from the surface and the summation is over all the ions in the solution. No simple analytical solution exists for the Poisson–Boltzmann equation. The Debye–Hückel theory of the electric double layer considers the limit when $Z_i e\psi \ll \kappa_B T$ such that the Poisson–Boltzmann equation can be linearized as

$$-\varepsilon_0 \varepsilon_r \nabla^2 \psi = \sum_i Z_i e n_{0i} \left(1 - \frac{Z_i e \psi}{\kappa_B T}\right) \tag{9.60}$$

Far away from the surface, the liquid has no net charge. This requires $\sum_i Z_i e n_{0i} = 0$. We further consider a planar geometry as shown in figure 9.7(a) such that eq. (9.60) can be written as

$$\frac{d^2\psi}{dx^2} = \psi \sum_i \frac{Z_i^2 e^2 n_{0i}}{\varepsilon_0 \varepsilon_r \kappa_B T} \tag{9.61}$$

with the boundary conditions

$$x = 0, \psi = \psi_s \text{ and } x \to \infty, \psi \to 0 \tag{9.62}$$

The solution for the potential distribution is then

$$\psi(x) = \psi_s e^{-x/\delta} \tag{9.63}$$

where δ is called the Debye length,

$$\frac{1}{\delta} = \sqrt{\sum_i \frac{Z_i^2 e^2 n_{oi}}{\varepsilon_0 \varepsilon_r \kappa_B T}} \tag{9.64}$$

which is very similar to the p–n junction width given by eq. (8.96). In fact, the development of p–n junction theory also relies on solving the Poisson–Boltzmann equation and exploited extensively the Debye–Hückel theory for the electric double layer (Shockley, 1949). The Debye length is of the order of a few nanometers for typical electrolytes, but can extend to hundreds of nanometers, depending on the dielectric constant and the ion concentration.

Now we consider the force balance inside the liquid. Because the liquid is stationary, the electrostatic force on the liquid must balance the pressure force. For the one-dimensional geometry in figure 9.7(a), this leads to

$$-\frac{dp}{dx} + \rho_n \left(-\frac{d\psi}{dx}\right) = 0 \tag{9.65}$$

where $(-d\psi/dx)$ gives the electric field and $\rho_n(-d\psi/dx)$ gives the electrostatic force. Again, substituting in the Boltzmann distribution for charge, we can write the above equation as

$$dp = -d\psi \sum_i Z_i e n_{0i} \exp\left(-\frac{Z_i e\psi}{\kappa_B T}\right) \tag{9.66}$$

The above equation can be integrated, from infinity where $p = p_\infty$ and $\psi = 0$, leading to

$$\begin{aligned} p(x) - p_\infty &= \sum_i n_{0i}\kappa_B T\left[\exp\left(-\frac{Z_i e\psi(x)}{\kappa_B T}\right) - 1\right] \\ &= \sum_i \kappa_B T\left[n_i(x) - n_{0i}\right] \end{aligned} \tag{9.67}$$

The right-hand side of eq. (9.67) is always positive and thus the pressure inside the electric double layer is higher than that inside the bulk liquid at the equilibrium state. When the surface potential is negative, the anion concentration in the liquid near the surface is in excess of its equilibrium distribution far away from the surface and the cation concentration is smaller than its equilibrium distribution. The net effect is that the electric double layer creates an attraction force between the ions on the solid surface and the counterions in the liquid. This attractive electrostatic force is balanced by the positive pressure in the liquid.

Hence, when two solid surfaces are brought close to each other as shown in figure 9.7(b), a repulsive force develops between the two surfaces because the electrostatic force between the liquid and the solid surfaces no longer balances the positive pressure inside the liquid. A detailed exact solution for the symmetric surface case with only one type of counterions in the liquid has been obtained without invoking the Debye–Hückel approximation (Israelachvili, 1992). In this case, the potential distribution and the repulsive pressure between the two surfaces are given by

$$\exp\left(-\frac{Ze\psi}{\kappa_B T}\right) = \frac{1}{\cos^2 Kx} \tag{9.68}$$

$$p(D) = \kappa_B T n_0(D) = 2\varepsilon_0\varepsilon_r\left(\frac{\kappa_B T}{Ze}\right)^2 K^2 \tag{9.69}$$

where n_0 is the counterion number density at the middle plane when the two surfaces are separated by a distance D, and $1/K$ is of the same order as the Debye length. K and n_0 are determined by the surface charge density c_s,

$$-\frac{2\kappa_B TK}{Ze}\tan\left(\frac{KD}{2}\right) = \frac{c_s}{\varepsilon_0\varepsilon_r} \tag{9.70}$$

$$K^2 = \frac{(Ze)^2 n_0}{2\varepsilon_0\varepsilon_r\kappa_B T} \tag{9.71}$$

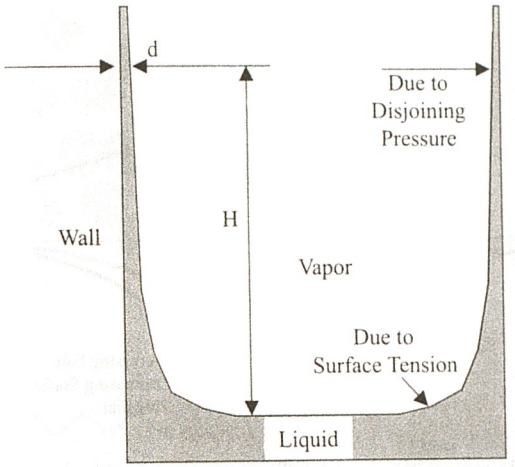

Figure 9.8 A repulsive disjoining pressure in a liquid film can raise the liquid film much higher than can surface tension.

As an example, consider two charged surfaces with $c_s = 0.2\,\mathrm{C\,m^{-2}}$ (which is one charge per 0.6 $\mathrm{nm^2}$) separated by $D = 2$ nm of water. Assuming monovalent counterions, that is, $Z = 1$, eq. (9.70) gives $K = 1.34 \times 10^9\ \mathrm{m^{-1}}$ and eq. (9.69) gives $p(D) = 1.7 \times 10^6\ \mathrm{N\,m^{-2}}$ or 17 atm. On the other hand, the van der Waals attraction force between the two surfaces, based on figure 8.5, is only $A/(12\pi D^3) \approx 3 \times 10^4\ \mathrm{N\,m^{-2}}$ for a typical Hamaker constant of 10^{-20} J, which is much smaller than the repulsive force of the electrical double layer.

The repulsive force inside the liquid, due to the electric double layer for the case discussed here and also due to a van der Waals force (when the Hamaker constant is negative), leads to the concept of disjoining pressure (Derjaguin et al., 1987). The repulsive force means that medium 3, in between media 1 and 2, experiences an expansion, or a negative pressure, which is superimposed onto normal compressive pressure. This disjoining pressure can result in a variety of consequences that may affect thin-film spreading and phase-change processes (Israelachvili, 1992; Wayner, 1998).

Figure 9.8 shows an example where the disjoining pressure plays an important role. The vapor–liquid interface can be thought of as the plane of symmetry in figure 9.7(b) if the additional liquid–vapor interface charge adsorption is neglected. The corresponding repulsive pressure (disjoining pressure) inside the liquid layer due to the electric double layer between the liquid–solid interface can be calculated from eq. (9.69) by taking $D = 2d$, where d is the liquid film thickness. In the limit of high surface charge density c_s, eq. (9.70) leads to the solution $K \to \pi/D$ and thus

$$p_d(d) = 2\varepsilon_0\varepsilon_r\left(\frac{\pi\kappa_B T}{2Zed}\right)^2 \tag{9.72}$$

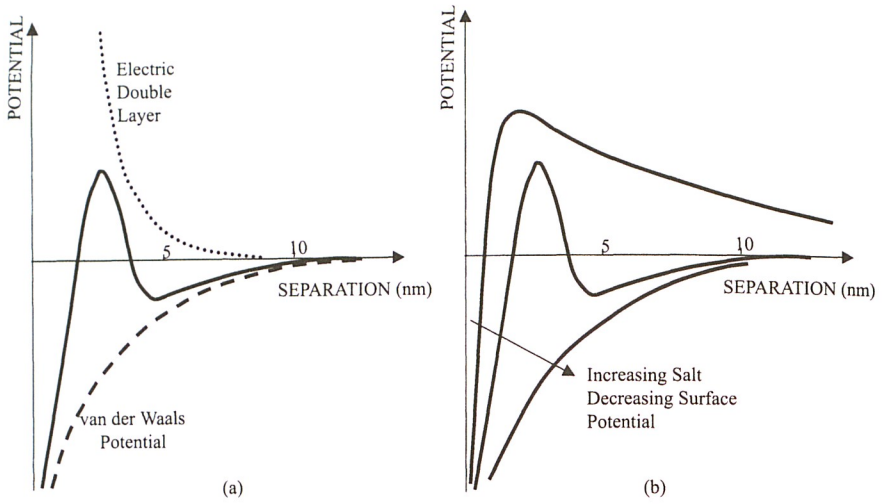

Figure 9.9 (a) Superposition of the double layer potential and van der Waals potential (DLVO theory). (b) Combined potential under varying salt concentration and surface potential.

This is known as the Langmuir equation. This repulsive pressure sucks the liquid film to a height H. At steady state, this liquid film is balanced by the gravitational force, $\rho_d g H$, which leads to

$$H = \frac{2\varepsilon_0 \varepsilon_r}{\rho_d g} \left(\frac{\pi \kappa_B T}{2Zed} \right)^2 \tag{9.73}$$

where ρ_d is the density of the liquid.

Combining the discussion in this section with that in the previous one, we see that the interaction potential between two close surfaces separated by a liquid layer experiences both electrostatic and van der Waals force,

$$\psi = \psi(\text{van der Waals}) + \psi(\text{electric double layer}) \tag{9.74}$$

The van der Waals force is usually attractive, although repulsive force can occur for some combinations of surfaces. The electric double layer generates a repulsive force. One possible combined potential profile between two surfaces is illustrated in figure 9.9(a). Whether the maximum or minimum in the figure appears or not apparently depends on the strength of each potential component. Unlike the interatomic potential, which has a short-range electrostatic repulsive force and a long-range van der Waals force, the electrostatic repulsive force due to a double layer is fairly long range. If the van der Waals potential between surfaces is attractive, it tends to pull the surfaces toward each other, whereas the repulsive electric double layer force prefers the separation of the solid surfaces.

To make the discussion more concrete, we consider a particulate solution. The balance between these two forces determines whether the particles form a stable solution (a colloid) or aggregate. For highly charged particles in a dilute electrolyte, there is a strong long-range repulsion that peaks at some distance (1–4 nm), creating an energy

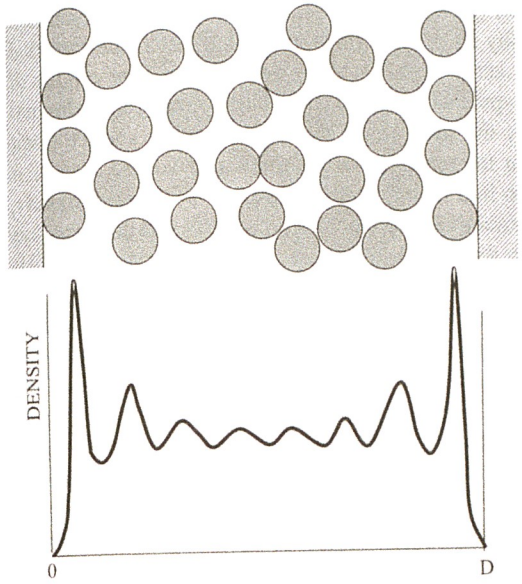

Figure 9.10 Illustration of density profile of liquids confined between two walls.

barrier [figure 9.9(b)]. In more concentrated electrolytic solutions, a secondary minimum forms before the energy barrier due to the decreased Debye layer thickness. This secondary minimum, although only marginally thermodynamically favorable, forms a metastable state of the particles, or a colloid. If the surface charge density is low, the repulsive potential is small and no energy barrier forms. In this case, the van der Waals force dominates and pulls the particles together. This aggregation process is also called coagulation or flocculation. This picture of colloids is called the DLVO theory, after Derjaguin and Landau (1941) and Verwey and Overbeek (1948).

9.2.4 Surface Forces and Potentials Due to Molecular Structures

The above analysis of the van der Waals force and the electric double layers are essentially a continuum approach that ignores the detailed molecular structure at the interfaces or the structures of the interfaces themselves. Within a few molecular layers of the interface, the molecular and interfacial structures alter the behavior of the interfacial potential.

Close to solid–liquid surfaces, the liquid molecules are more regularly arranged because of the constraints of the immobile solid atoms. The density profile oscillates as shown in figure 9.10. This density variation causes an oscillatory pressure variation, called the solvation force, that is superimposed onto the van der Waals and electric double layer forces based on the continuum analysis. As indicated in figure 9.10, the structural variations occur only within a few (~3) molecular layers near the surface, as does the oscillatory solvation force. Consequently, as two surfaces are brought close together, the pressure between the two surfaces varies (Israelachvili, 1992; Koplik and Banavar, 1995). In addition to the oscillatory solvation force,

a repulsive force exists between two hydrophilic surfaces and is called the hydration force. The force decays exponentially from the surface at a much faster rate than that of the electric double layer and is active within a range of 1–5 nm. The origins of this hydration force are either the repulsive nature of the similarly charged hydrogen-bonding surface groups that modify the structure of the water near the surface (their effective range is about 3–5 nm), or the repulsion of the thermally excited molecular chains protruding from one medium into the other (their range is 1–2 nm). Similarly, between hydrophobic surfaces, an attractive hydrophobic force exists and this force has a range of ~10 nm and can be much stronger than that predicted for the van der Waals attraction force.

It is assumed in the above discussions that the interacting surfaces are well defined, rigid, and smooth. At liquid–liquid, and liquid–vapor interfaces, thermal fluctuation changes the interface constantly, and this can be considered as a roughness of the interface. Similarly, liquid–polymer and polymer–polymer interfaces are also "rough" to the size of the polymers. As two such surfaces come together, a repulsive force develops, due to either the confinement of the motion of each interface (fluctuation force) or the interaction of the molecules (steric force). These repulsive forces are often understood from the configurational entropy perspective. For a more detailed discussion on these forces, refer to the excellent textbook by Israelachvili (1992).

9.2.5 Surface Tension

At a liquid–vapor interface, the atoms experience a different potential from those atoms deep inside the liquid, and a similar argument can also be made for solid–vapor and solid–liquid interfaces. The liquid molecules at the interface have the tendency to escape to the vapor side and the intermolecular spacing at the interfaces is larger than deep inside the liquid. This causes an effective density variation, as illustrated in figure 9.11. The larger intermolecular distance also means that the molecules at the interfacial region have a higher potential energy than those inside. The excess energy needed to bring the liquid molecules from inside the liquid to the interfacial region, per unit area of the interface, is the surface tension γ, or the energy "cost" of creating the surface. The surface tension units are [J m^{-2}], or [N m^{-1}] in the more familiar force unit. This force unit is also related to the conventional understanding of surface tension as the tangential force along the interface per unit length. Under this force picture, the work required to stretch a liquid membrane as shown in figure 9.12 is

$$W = \int F\,dx = \int 2\gamma L\,dx = 2\gamma L\,\Delta x = \gamma \Delta A_s \tag{9.75}$$

where ΔA_s is the total surface area increase and the factor of two arises from the existence of two interfaces of the membrane. During this stretching, the liquid molecules inside the membrane are pushed toward the interfaces. In thermodynamics, work is a path dependent variable. However, the surface tension is a thermodynamic variable, analogous to the pressure in bulk fluids (Defay et al., 1966; Hiemenz, 1986). Equation (9.75) is similar to the $p\Delta V$ work in bulk fluids due to volume expansion. In fact, the analogy between surface layer and bulk fluid extends far beyond surface tension and pressure. Surface states are important topics in colloidal and surface chemistry.

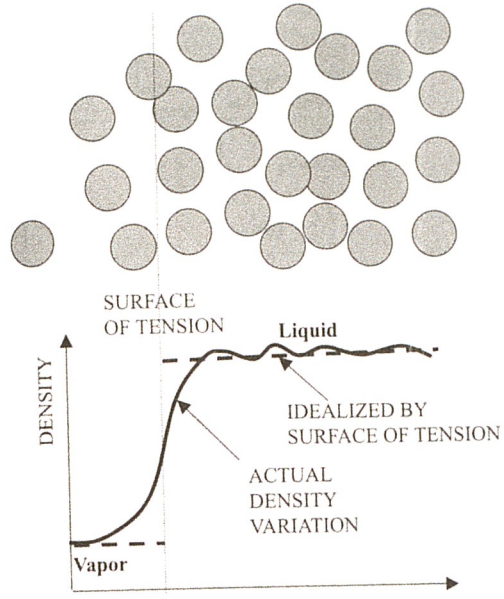

Figure 9.11 Density variation near a liquid–vapor interface. The surface of tension is an idealized plane that divides the interfacial region into the vapor side and the liquid side. On each side, bulk properties of liquid and vapor apply up to the surface of tension.

The bulk equations of states and fluid flow all have analogies for two-dimensional surfaces, which will not be discussed further (Hiemenz, 1986).

The surface tension concept approximates the interface as a mathematical plane (figure 9.11)—the surface where the tension acts, which sharply divides the liquid and the vapor. On each side of the surface of tension, the properties are assumed to be uniform and equal to that of the bulk values on the same side. The physical interface between liquid and vapor phases, however, is not sharp, as figure 9.11 indicates, with the density varying from that of the liquid to that of the vapor over a narrow range. The exact location of the surface of tension, however, depends on definition. Young (1972) defines the surface of tension on the basis of the mechanical force balance, whereas the Gibbs (1928) treatment, based on thermodynamics, defines the surface (Gibbs surface) as the location where the liquid and the vapor are of equal molar concentration. Here,

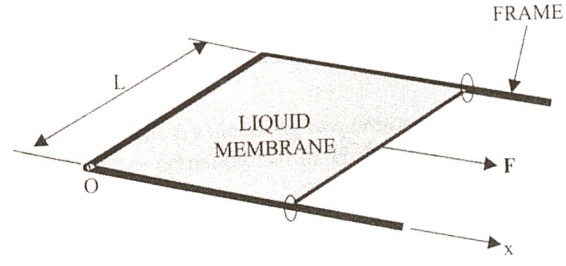

Figure 9.12
Stretching of a liquid membrane.

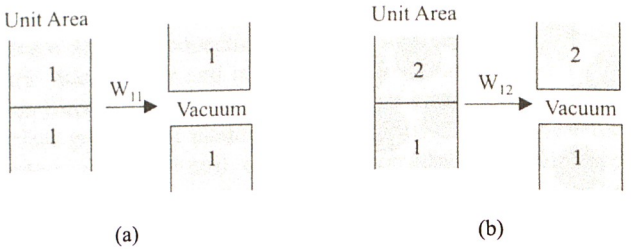

Figure 9.13 (a) Work of cohesion W_{11} is the energy needed to create two surfaces of unit area from the same matter. (b) Work of adhesion W_{12} is the energy needed per unit area to separate two different surfaces in contact.

we will not get into details of these discussions but refer interested readers to references on this topic (Defay et al., 1966; Hiemenz, 1986).

Theoretically, the surface tension can be determined from the interfacial potential discussed earlier. We consider first the separation of a solid into two parts, separated by a vacuum, as shown in figure 9.13(a). The energy needed per unit area, or the work done to separate the solid, is called the work of cohesion W_{11}. After separation, two surfaces are formed. The energy input during the separation of the solid is stored at the two surfaces, and thus the surface tension is

$$\gamma_1 = \frac{1}{2} W_{11} \tag{9.76}$$

For liquids, we cannot directly use this process to create two surfaces physically. However, we can increase the area of an existing surface easily. The energy needed per unit increase in the surface area is the surface tension, which can be similarly calculated from eq. (9.76) if we imagine that liquid can be similarly separated. To evaluate W_{11}, we can refer to figure 9.6 for the van der Waals force interaction between atoms in the medium. The work done in separating two parallel plates from a separation of D to infinity is

$$W_{11d} = \frac{A}{12\pi D^2} \tag{9.77}$$

where we have used the superscript d to denote that this is due to van der Waals, or the London dispersion potential. When the two media are in contact, the effective separation $D \approx \sigma/2.5$. For a typical value of $\sigma = 0.4$ nm, $D \approx 0.16$ nm. Substituting this value into eqs. (9.77) and (9.76), we obtain

$$\gamma_1 \approx \frac{A}{24\pi}(0.16\,\text{nm})^{-2} \tag{9.78}$$

This simple estimation based on $D = 0.16$ nm actually gives very good values of surface energy for a wide variety of solid and liquid surfaces, as shown in Table 9.1.

Now consider the separation of two immiscible liquids in contact into two stand-alone parts at the interface [figure 9.13(b)]. After separation, the interfacial energy on each

Table 9.1 Hamaker constant and surface tension of typical fluids

Material	Theoretical Hamaker Constant (10^{-20} J)	Surface Tension (mN m^{-1})	
		Eq. (9.78)	Experimental
Liquid helium	0.057	0.28	0.12–0.35
n-pentane	3.75	18.3	16.1
n-octane	4.5	21.9	21.6
CCl_4	5.5	26.8	29.7
Acetone	4.1	20	23.7
Ethanol	4.2	20.5	22.8
Methanol	3.6	18	23
Glycol	5.6	28	48
Glycerol	6.7	33	63
Water	3.7	18	73

Source: Israelachvili, 1992.

surface is γ_1 and γ_2. The energy difference between the surface energy after separation and the interfacial tension γ_{12} before separation is called the work of adhesion,

$$W_{12} = \gamma_1 + \gamma_2 - \gamma_{12} \tag{9.79}$$

The above is the Dupré equation, which leads to a way of calculating the surface tension γ_{12}. The work of adhesion can be approximately estimated from the work of cohesion,

$$W_{12} = \sqrt{W_{11d} W_{22d}} = 2\sqrt{\gamma_{1d}\gamma_{2d}} \tag{9.80}$$

Equations (9.79) and (9.80) lead to

$$\gamma_{12} = \gamma_1 + \gamma_2 - 2\sqrt{\gamma_{1d}\gamma_{2d}} \tag{9.81}$$

Equation (9.81) is often called the Girifalco–Good–Fowkes equation. The square root term is due to the London dispersion force (van der Waals force), while $(\gamma_1 + \gamma_2)$ includes all mechanisms contributing to the interfacial potential, on the basis of the argument that only the van der Waals potential operates across the interface.

Consider now a curved interface, figure 9.14. Because the surface tension is tangential to the surface, it has a component pointing toward the concave side of the interface, which must be balanced by a pressure difference across the surface. The normal force component due to the pressure difference is

$$(p'' - p')\Delta x \Delta y$$

where Δx and Δy are along two orthogonal directions. The surface tension force along the two lines perpendicular to length Δx is $\gamma \Delta x$, and its normal force component is

$$2\gamma \Delta x \sin(\Delta\theta_y) = 2\gamma \Delta x \times \Delta\theta_y = 2\gamma \Delta x \frac{\Delta y}{2r_y} \tag{9.82}$$

where r_y is the radius of curvature for the curve Δy. A similar expression exists for the force component along the two lines perpendicular to Δy. Equating the normal

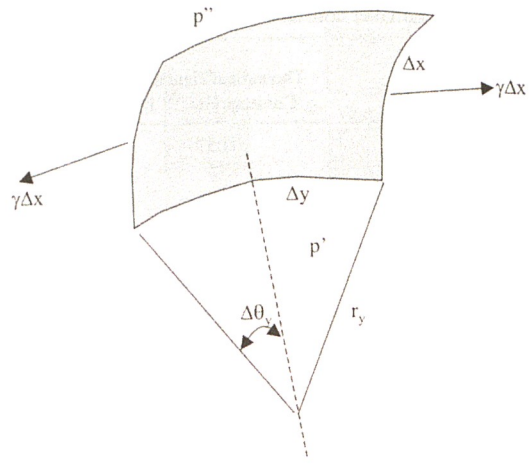

Figure 9.14 Derivation of Laplace equation for pressure difference created due to surface tension on a curved surface.

pressure force to the projection of the surface tension force, we obtain the Laplace equation

$$p'' - p' = \gamma \left(\frac{1}{r_x} + \frac{1}{r_y} \right) \tag{9.83}$$

where r_x and r_y are the two local radii of curvature in two orthogonal directions, usually taken along the principal directions of the surface such that r_x and r_y are the principal radii of curvature. For a spherical surface, $r_x = r_y = r$, the Laplace equation becomes

$$p'' - p' = \frac{2\gamma}{r} \tag{9.84}$$

When a liquid condenses on a solid surface, there are three phases and potentially three interfaces, the liquid–vapor, the liquid–solid, and the solid–vapor. Knowing the interfacial tension for each interface, we can use a simple force balance to derive the static contact angle between a droplet and a surface as shown in figure 9.15,

$$\gamma_{13} = \gamma_{23} \cos\theta + \gamma_{12} \tag{9.85}$$

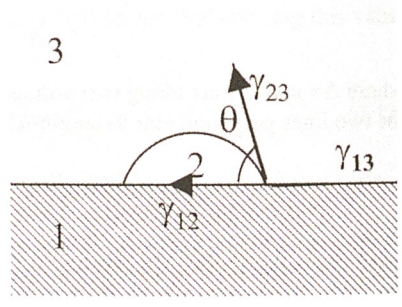

Figure 9.15 Derivation of the Young equation.

which is known as the Young equation. Depending on the values of surface tension at the three interfaces, a solution for θ may exist. In this case, the liquid forms droplets on the surface. When there exists no solution for θ, the liquid film spreads out to wet the surface.

9.3 Size Effects on Single-Phase Flow and Convection

The above discussion suggests that in the range of a few to tens of nanometers, and maybe even hundreds of nanometers in the case of the electric double layer (depending on the Debye length), the intermolecular potential between liquid molecules and liquid–solid surfaces may be modified. These modifications can potentially impact the fluid flow and heat transfer characteristics in micro- and nanostructures. Up to now, however, there exists no simple way to estimate how the interfacial potential affects fluid flow and heat transfer characteristics. The experimental data on pressure-driven fluid flow in microchannels scatter widely and lead to different interpretations, and not much data are available for nanochannels. In this section, we will first comment on pressure-driven flow in micro- and nanoscale channels, then follow with a brief introduction to electrokinetic and electrophoretic flows. The latter is much better understood and widely used in biotechnology.

9.3.1 Pressure-Driven Flow and Heat Transfer in Micro- and Nanochannels

Developments in micro-electro-mechanical systems (MEMS) have attracted strong interest in fluid flow and heat transfer in microchannels (Ho and Tai, 1998). Quite a large amount of experimental work has been performed on fluid flow in microchannels, particularly in relation to applications in biotechnology. Theoretically, one question that has been debated is whether fluid flow in microchannels deviates from the laws used for macrochannels. Unfortunately, experimental work so far has not been conclusive. The earliest experiments on liquid flow in microchannels were carried out by Poiseuille [see Sutera and Skalak, (1993) for an interesting historical review]. Poiseuille was interested in blood flow in the arterioles and venules but realized that controlled experiments using simple liquids would give him clearer formulations of the laws governing blood flow. His experiments employed glass tubes with diameters in the range of 15–600 μm and lengths of 6.77–100.5 mm. Many fluids were tested, including water, aqueous salt solutions, teas, wines and spirits, extracts of plants and roots, ethers, alcohols, and solutions of ammonia. On the basis of these experiments, he derived the following expression for the volumetric flow rate,

$$Q_V = \frac{\pi D^4 \Delta P}{128\, \mu L} \tag{9.86}$$

which we now call the Poiseuille law. In eq. (9.86), D is the tube diameter, L is the length of the tube, and ΔP is the total pressure drop.

At the time of Poiseuille's experiments, the concept of viscosity was just being developed and was not used in his work. Yet the viscosity values deduced from his

experimental data are within 0.1% of the accepted values! These facts strongly suggest that liquid flow in microchannels of comparable diameter should not deviate significantly from predictions of the classical laws. However, some recent experiments in microchannels of comparable or even larger diameters indicate deviations from Poiseuille's results. What are the possible reasons for the deviation observed in recent experiments? Examining these experiments, we can infer the following causes:

1. *Entrance and exit region effects.* In Poiseuille's experiments, the entrance region was carefully shaped and the exit was situated in water to eliminate the effects of surface tension at the exit. Long tubes were used such that the entrance region was much shorter than the fully developed flow. More recent experiments using silicon or stainless steel microchannels usually do not allow similar precautions to be taken for the entrance and exit effects.
2. *Surface roughness effects.* Stainless steel tubes and micromachined channels typically have a surface roughness larger than that of blown glass tubes. There exist observations of early transition to turbulence and deviation from the Moody friction factor chart in microchannels. Although the simple scaling law based on relative surface roughness to the diameter seems to be sufficient for the modification of the friction factor in macrochannels, one may argue that this may not be the most appropriate parameter in a microchannel. For example, with decreasing diameter the volume-to-surface ratio of the liquid in contact with the wall decreases. How does such a ratio influence the friction factor for microchannel flow is an open question.
3. *Effects of surface forces.* Because the surfaces of silicon and stainless steel are different from that of glass, the surface forces discussed in section 9.2 may play a role in determining the friction factor or heat transfer characteristics. However, there is no modeling or simulation to quantify the effects of surface forces on single-phase flow.
4. *Experimental error.* Because fluid flow in microchannels typically requires high pressure and the flow rate is very small, it takes a long time to reach steady state. An accurate characterization of the channel diameter is critical because the flow rate is proportional to $\sim D^4$.

Given the existing large variations that exist in reported fluid flow characteristics in microchannels, it is not strange to see a similarly large variation in the experimental data on heat transfer characteristics in such channels (Obot, 2000; Sobhan and Garimella, 2000). Despite these large variations, consensus is gradually emerging that these variations are more likely to be due to causes similar to those listed above rather than the breakdown of the continuum approximation.

Moving further down in scale, fluid flow in nanoscale becomes of interest to the understanding of a wide range of phenomena, such as self-assembly, DNA dynamics in liquids, and nanofabrication. The extreme of very narrow channels is amenable to molecular dynamics simulation, as reviewed by Koplik and Banavar (1995). One question on which molecular dynamics can provide considerable insight is that of boundary conditions. Koplik et al. (1989) concluded that, in a simple liquid undergoing Poiseuille or Couette flow, for all practical purposes the average velocity vanishes at the wall and thus the non-slip boundary conditions are valid. Thompson and Robbins (1990) showed that in-plane ordering is a key factor in being able to transmit shear stress across the fluid–solid interface. By varying the temperature, the wall–fluid commensurability, and the wall–fluid couplings, the range of behaviors from complete slip to non-slip

was observed in their simulations. For simple spherical molecules, a direct correlation between the extent of in-plane ordering and the degree of slip was found. A general boundary condition was proposed, based on molecular dynamics simulation of Couette flow using the Lennard–Jones potential (Thompson and Troian, 1997). So far, there have not been many studies on convective heat transfer in nanochannels, despite the fact that molecular dynamics has been widely used to study phase change and heat conduction problems.

Example 9.3 *Order of magnitude for slip to occur*

To estimate the order of magnitude for the slip to occur, we consider a simple model as shown in figure E9.3(a). A molecule sits on top of a plane of molecules forming a solid surface. Estimate how much shear force is needed to slide the molecule on the surfaces.

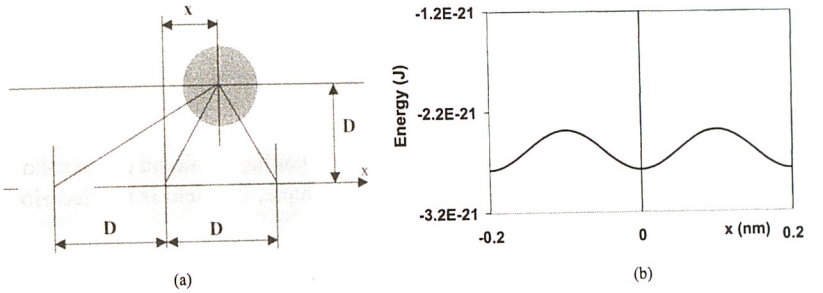

Figure E9.3 Figure for example 9.3.

Solution: We consider the van der Waals attraction potential between the molecule of interest and the solid wall. Assuming that the distance between the molecule and the surface is D, the interaction potential as a function coordinate x is then

$$\Phi(x, y) = -\sum_{i=-\infty}^{\infty} \frac{C}{[D^2 + (iD - x)^2 + (jD - y)^2]^3} \tag{E9.3.1}$$

where y is the coordinate direction perpendicular to the page. In figure E9.3(b), we plotted the above expression using typical values of $D(= 0.2$ nm) and C (10^{-77} J m^6) as a function of x for $y = 0$. From the potential distribution, the attraction force acting on the molecule can be estimated, which is $\sim 10^{-11}$ N. Considering that there is approximately one molecular per (0.2 nm)^2 of surface area, the shear stress needed to cause the layer of molecules to slip is then $\sim 10^{10}$ N m^{-2}. To put this value into perspective, the shear stress generated for a velocity change of 1 m s^{-1} over 1 μm is 10^3 N m^{-2} using the viscosity of water. These numbers strongly suggest that the slip flow is unlikely to occur.

Comments. The above model is very crude. It does not include the interaction of the molecules with the other molecules and does not include the thermal motion of the molecules. We encourage interested readers to develop more rigorous models along similar lines of reasoning.

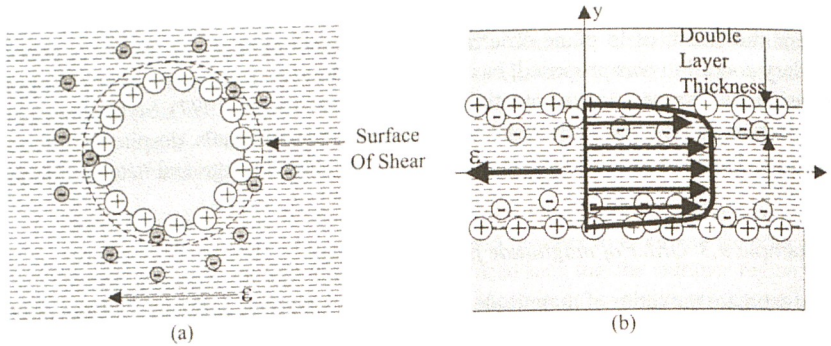

Figure 9.16 Electrokinetic phenomena: (a) electrophoresis; (b) electro-osmosis.

9.3.2 Electrokinetic Flows

The electrical double layer discussed in section 9.2.3 can be exploited to create various kinds of flows that have become increasingly important for micro- and nanofluidic devices. Under an external electrical field, positively and negatively charged particles experience forces in opposite directions, which may set either the liquid or the solid into motion, depending on their relative mobility. For example, if a field is applied along a stationary dielectric solid wall with an electric double layer, the ions in the liquid side experience an electrostatic force and are set into motion. These ions will drag the bulk liquid into motion through viscous force (Rice and Whitehead, 1965). Such fluid flow phenomena are known as electro-osmosis [figure 9.16(b)]. In other situations, such as when particles are suspended inside an electrolyte, an external electric field can set the charged particles into motion, a phenomenon called electrophoresis [figure 9.16(a)].

9.3.2.1 Electrophoretic Motion

As an example of electrophoresis, we consider the motion of a charged sphere inside an electrolytic solution under an external electric field $\mathscr{E}$, as shown in figure 9.16(a). The particle experiences a force and will be set into motion. A layer of liquid molecules in the immediate vicinity of the particle will also move at the same velocity as the particle due to the strong molecular bonding between the solid and the liquid molecules. This layer is typically only a few atomic layers thick but it affects the net charge and thus the electrostatic force on the particle [similar to the Stern layer in figure 9.7(a)]. The boundary between this immobile liquid layer and the mobile liquid molecules is called the surface of shear and its location is generally difficult to determine exactly. The balance of the electrostatic force with the viscous force leads to

$$3\pi\mu D\mathbf{u} = q\mathscr{E} \text{ or } \mathbf{u} = \frac{q\mathscr{E}}{3\pi\mu D} \tag{9.87}$$

where $\mathbf{u}$ is the drift velocity of the particle relative to the solution. The charge on a particle q should be considered as the net charge within the surface of shear. It can be related to the electrostatic potential at the surface of shear, which is also called the zeta

potential (ζ), by solving the Poisson–Boltzmann equation for a spherical coordinate. When the Debye layer thickness δ is much larger than the particle diameter, the zeta potential is (Hiemenz, 1986)

$$\zeta = \frac{q}{2\pi\varepsilon_0\varepsilon_r D}\frac{\delta}{\delta + D/2} \approx \frac{q}{2\pi\varepsilon_0\varepsilon_r D} \tag{9.88}$$

Substituting eq (9.88) into (9.87) leads to an expression of the particle velocity in terms of the zeta potential,

$$\mathbf{u} = \frac{2\zeta\varepsilon_0\varepsilon_r\mathscr{E}}{3\mu} \tag{9.89}$$

The above analysis can be applied to biomolecules. Different biomolecules (DNAs and proteins) usually have different charge and effective diameters and thus will have different terminal velocities. Under the same electric field, they have different drift velocities and thus travel different distances, which means that different biomolecules can be separated. This is the basis of gel-electrophoresis, which is widely used in biology to separate biomolecules (Manchenko, 2003).

9.3.2.2 Electro-Osmotic Flow

We consider now the electrostatically driven osmotic fluid flow in microchannels formed between two parallel plates as shown in figure 9.16(b). Taking a differential control volume of the fluids, the balance of the viscous force and the electrostatic force gives

$$\mu\frac{d^2u}{dy^2} = \rho_n\mathscr{E}_x = \mathscr{E}_x\left(-\varepsilon_0\varepsilon_r\frac{d^2\psi}{dy^2}\right) \tag{9.90}$$

where $\mathscr{E}_x$ is the x component of the electric field. This equation should be coupled to the Poisson–Boltzmann equation to obtain the potential profile. Here we assume that the thickness of the electric double layer δ is small compared to the plate spacing; that is, $\delta \ll D$. Outside the electric double layer, $\psi = 0$ and thus eq. (9.90) becomes

$$\mu\frac{d^2u}{dy^2} = 0 \text{ for } -\left(\frac{D}{2} - \delta\right) \le y \le \left(\frac{D}{2} - \delta\right) \tag{9.91}$$

The above equation can be integrated once to give

$$\mu\frac{du}{dy} = C_1 \tag{9.92}$$

The symmetry requirement at $y = 0$ leads to $C_1 = 0$. Thus the velocity distribution must be a constant outside the electric double layer,

$$u(y) = u_0 \text{ for } -\left(\frac{D}{2} - \delta\right) \le y \le \left(\frac{D}{2} - \delta\right) \tag{9.93}$$

Now consider transport inside the electric double layer. Integrating eq. (9.90) once leads to

$$\mu \frac{du}{dy} = -\varepsilon_0 \varepsilon_r \mathscr{E}_x \left(\frac{d\psi}{dy} \right) + C_2 \tag{9.94}$$

At the edge of the electric double layer, $du/dy = 0$ and $d\psi/dy = 0$, thus $C_2 = 0$. Integrating eq. (9.94) again, from the wall to the edge of the electric double layer, we have

$$\mu[u_0 - u(y = -D/2)] = -\varepsilon_0 \varepsilon_r \mathscr{E}_x [\psi(y = -D/2 + \delta) - \zeta] \tag{9.95}$$

where ζ is the zeta potential on the surface of the shear (we have neglected the thickness of the surface of the shear). At the edge of the electric double layer, $y = -D/2 + \delta$, the potential ψ is zero. On the surface of the shear, the velocity is zero. Thus, eq. (9.95) gives the velocity of the fluid in the center region of the channel as

$$u_0 = \frac{\varepsilon_0 \varepsilon_r \mathscr{E}_x \zeta}{\mu} \tag{9.96}$$

The velocity profile of an electro-osmotic flow is sketched in figure 16(b). Because the electric double layer thickness is much smaller than the plate separation, the flow is essentially a plug flow with uniform velocity. Within the electric double layer, the velocity decreases continuously to zero at the surface of the shear.

The above derivation of electro-osmotic flow does not consider the fluid structure near the surfaces such as that sketched in figure 9.10. A recent molecular dynamics study (Freund, 2002) found that ions are more attracted to the wall than the Poisson–Boltzmann equation predicts for electro-osmotic flow in nanochannels, suggesting that discrete nature of ions can be important for flow in nanostructures.

9.4 Size Effects on Phase Transition

Size has profound effects on phase change processes. One can easily appreciate this from the Laplace equation, eq. (9.84), that shows pressure dependence on curvature. Since pressure is related to other thermodynamic properties, it is reasonable to anticipate that certain thermodynamic properties will be influenced by size. Examples are surface tension, phase transition pressure and temperature, and so on. In-depth discussion of the thermodynamics of small systems can be found in the work of Hill (1963, 1964). Here we focus on the effects of curvature. We further limit our discussion to the phase transition of a pure substance; in other words, only one material exists in the system so that only two phases are present.

The starting point in analyzing curvature effects on thermodynamic properties is based on the Laplace equation and thermodynamic relations. We consider a spherical geometry (droplet or bubble). The inner pressure is p″ and the surrounding fluid pressure is p′. When the system goes from one equilibrium state to another, the Laplace equation (9.84) leads to

$$dp'' - dp' = d\left(\frac{2\gamma}{r} \right) \tag{9.97}$$

Next, we eliminate some variables so that we can solve the above equation. Because each phase is in thermal equilibrium, we can use the Gibbs–Duhem equation [eq. (8.83)] for each of the bulk phases

$$s'dT - v'dp' + d\mu' = 0 \tag{9.98}$$

$$s''dT - v''dp'' + d\mu'' = 0 \tag{9.99}$$

where s and v are the entropy and volume per mole, respectively, and μ is the chemical potential. A similar equation, called the Gibbs equation, exists for the interface,

$$d\gamma = -s_i dT - \Gamma d\mu_i \tag{9.100}$$

where Γ is the number density of molecules per unit area at the surface of tension, s_i is the entropy per unit area, and μ_i is the chemical potential at the interface. Equations (9.97)–(9.100) form the basis for analysing the effects of curvature on thermodynamic properties. Which of the variables we choose to eliminate depends on whether the liquid or the vapor is inside the sphere, and what are the system constraints, that is, constant pressure or constant temperature. We discuss a few cases below.

9.4.1 Curvature Effect on Vapor Pressure of Droplets

First we consider a droplet system at constant temperature so that p'' is the pressure inside the liquid droplet. At equilibrium, since $\mu' = \mu'' = \mu_i = \mu$, eqs. (9.98) and (9.99) lead to

$$v'dp' = v''dp'' \tag{9.101}$$

Substituting eq. (9.101) into (9.97) and eliminating p'' yields

$$d\left(\frac{2\sigma}{r} \right) = \frac{v' - v''}{v''} dp' \tag{9.102}$$

If we further assume $v' \gg v''$, the ideal gas law for the vapor phase, and that v'' (liquid) is independent of pressure, the above equation can be integrated, leading to the Kelvin equation

$$\ln\left(\frac{p'}{p_0} \right) = \frac{2\sigma}{r} \frac{v''}{RT} \tag{9.103}$$

where R is the universal gas constant and p_0 is the normal vapor pressure when the interface is flat ($r \to \infty$). This equation shows that the equilibrium vapor pressure increases as the liquid droplet radius decreases. For a given vapor pressure, smaller droplets tend to evaporate. Thus, in a mist of droplets of pure substance, the large droplets will grow at the expense of the small droplets since they have a lower vapor pressure.

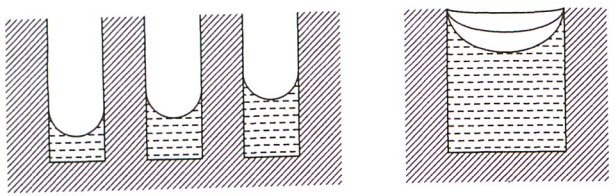

Figure 9.17 Capillary condensation inside nanopores. (a) Before the pores are filled, the vapor pressure inside the pores is lower than in bulk form; even superheated vapor may condense if eq. (9.104) is satisfied. (b) Once the meniscus reaches the mouth of the pore, the vapor pressure starts to increase as the radius of curvature decreases.

If, instead of droplets, bubbles are formed in a liquid ambient, a similar analysis leads to the Kelvin equation for the vapor pressure p'' in the bubble,

$$\ln\left(\frac{p''}{p_0}\right) = -\frac{2\gamma}{r}\frac{v'}{RT} \tag{9.104}$$

which shows that the equilibrium vapor pressure inside a bubble is lower than its corresponding equilibrium pressure when a flat interface exists.

We can use the Kelvin relation to understand the condensation of a vapor in a porous medium [figure 9.17(a) and (b)]. Let us first consider an idealized problem in which all the pores are cylinders of the same radius. We suppose that the pores are partially filled with a liquid in contact with its own vapor and assume furthermore that the walls of the pores are completely wetted by the liquid. So long as the menisci are away from the mouths of the pores, all the menisci will have hemispherical surfaces of radius r. The vapor pressure in the pores is given by eq. (9.104) and is less than p_0. Consequently, liquid can exist in a porous medium in equlibrium with superheated vapor. If the vapor pressure is increased slightly, condensation will occur in all pores in which the meniscus has not yet reached the mouth of the pore; further condensation would result in an increase of the radius of curvature of the surface. Condensation in this pore therefore ceases when the radius of curvature reaches the equilibrium value corresponding to the vapor pressure. Thus condensation will proceed in the partially filled pores and be halted in the filled pores, until a point is reached at which all the pores are similarly filled and the liquid in them has everywhere the radius of curvature corresponding to the vapor pressure. Further increase in the vapor pressure results in condensation in all the pores and the flattening of the menisci, which become plane when $p'' = p_0$. The vapor is now saturated and any further increase in p'' is immediately offset by condensation of bulk liquid.

This reduced vapor pressure when the vapor is on the concave side and the increased vapor pressure when the vapor is on the convex side may be related to some technologies being used in nanowire growth. One method developed, for example, is to condense vapors of materials onto a template (Heremans et al., 2000), such as anodized alumina, that can have channels with a diameter in the range of 10–200 nm. In this case, the Kelvin relation suggests that the vapor pressure inside the channels may be lower than that of the bulk saturation pressure and thus even superheated vapors may condense in very small channels. Another example is the vapor–liquid–solid growth of nanowires in free space (Morales and Lieber, 1998). In this case, vapor condenses on convex surfaces

which may have a higher vapor pressure that favors the growth of wires with bigger diameters. These possibilities, however, have not been studied experimentally, nor fully exploited in the control of nanowire growth.

9.4.2 Curvature Effect on Equilibrium Phase Transition Temperature

We now examine the size dependence of the equilibrium phase transition temperature. For this purpose, we will assume that the external pressure is constant, that is, $dp' = 0$ in eq. (9.98). In the case of droplets, we can subtract eq. (9.98) from (9.99) to obtain

$$\frac{\Delta h}{T}dT + v''dp'' = 0 \tag{9.105}$$

where $\Delta h = T(s' - s'')$ is the latent heat. Substituting eq. (9.105) into (9.97) leads to

$$\frac{dT}{T} = -\frac{v''}{\Delta h}d\left(\frac{2\gamma}{r}\right) \tag{9.106}$$

Integrating the above equation from $r \to \infty$ ($T = T_0$) to r, we obtain

$$\ln\frac{T}{T_0} = -\frac{2\gamma}{r}\frac{v''}{\Delta h} \tag{9.107}$$

This shows that the equilibrium temperature of small droplets is lower than that of a flat interface.

If, instead of droplets, bubbles are formed inside liquid under a constant liquid pressure, a slightly more complicated derivation, due to the compressibility of the vapor phase, leads to (Defay et al., 1956)

$$\overline{\Delta h}\left(\frac{1}{T_0} - \frac{1}{T}\right) = R\ln\frac{2\sigma/r + p'}{p'} \tag{9.108}$$

where $\overline{\Delta h}$ is the average latent heat in the range between T_0 and T. It should also be pointed out that the latent heat can also be size dependent and could be analyzed on the basis of the same sets of equations [see Defay et al. (1956) for details]. Equation (9.108) shows that the equilibrium temperature of small vapor bubbles must be higher than the normal phase transition temperature T_0, which explains the existence of superheated liquid.

9.4.3 Extension to Solid Particles

A similar analysis can be extended to small solid particles by replacing the liquid with the solid properties. Such an extension leads to the following conclusions:

1. The vapor pressure of small crystals is greater than that of large crystals. In the presence of vapor, large crystals will grow at the expense of smaller crystals.
2. Small crystals melt at a temperature lower than the bulk melting point. The melting point T of a small crystal is given by

$$\ln\frac{T}{T_0} = -\frac{2\gamma^{s\ell}}{r}\frac{v_s}{\Delta h_{s\ell}} \tag{9.109}$$

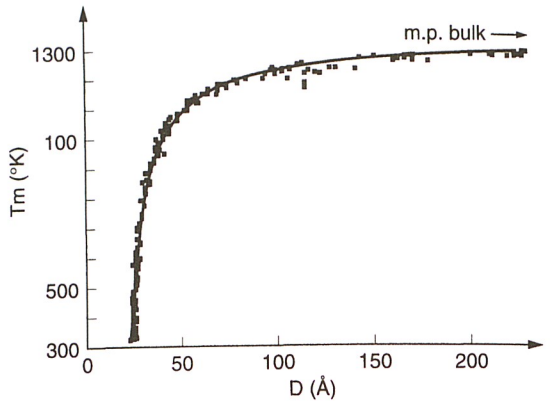

Figure 9.18
Experimental results on the melting point of gold nanoparticles as a function of the particle diameter (Buffat and Borel, 1976; courtesy of APS Associate Publisher).

where T_0 is the normal melting point at the same external pressure, $\gamma^{s\ell}$ is the interfacial tension at the solid–liquid interface, v_s is the molar volume of the solid, and $\Delta h_{s\ell}$ is the heat of fusion. A well-established example is the lowering of the melting point of gold nanoparticles, as shown in figure 9.18 (Buffat and Borel, 1976).

3. The melting point of a substance solidified in the pores of an inert material will depend on the size of the pores. For a more detailed discussion, see Defay et al. (1966).
4. Small crystals may have a heat of fusion and a heat of sublimation smaller than the value for bulk solid.

9.4.4 Curvature Effect on Surface Tension

The size dependence of surface tension has been under investigation since Gibbs (1928) but still remains a topic of debate. Tolman's (1949) work is a classic in this field. The Tolman theory treats a single-component system with two phases and uses the same set of equations (9.97)–(9.100). Considering a droplet at constant temperature, we have

$$d\left(\frac{2\gamma}{r}\right) = \frac{v' - v''}{v''} dp'' \tag{9.110}$$

or

$$\frac{2}{r} d\gamma + 2\gamma d\left(\frac{1}{r}\right) = \frac{v' - v''}{v''} dp'' \tag{9.111}$$

To eliminate dp'', we use eq. (9.100),

$$d\gamma = -\Gamma d\mu_i = -\Gamma v'' dp'' \tag{9.112}$$

From eqs. (9.111) and (9.112), we obtain

$$\frac{d\gamma}{\gamma} = -\frac{2\Gamma}{(2\Gamma/r) + \rho_d'' - \rho_d'} d\left(\frac{1}{r}\right) \tag{9.113}$$

where ρ_d'' and ρ_d' are the densities of the two phases.

For a liquid droplet, ρ_d' (the vapor side) is negligible and eq. (9.113) can be integrated to give

$$\frac{\gamma(r)}{\gamma_0} \approx \frac{1}{1 + (2\Gamma/\rho_d'')/r} \tag{9.114}$$

where γ_0 is the surface tension for a flat surface. Equation (9.114) shows that the surface tension of a droplet decreases with decreasing droplet diameter. For a vapor bubble inside a liquid, ρ_d'' (the vapor side) is negligible and eq. (9.113) leads to

$$\frac{\gamma(r)}{\gamma_0} \approx \frac{1}{1 - (2\Gamma/\rho_d')/r} \tag{9.115}$$

and thus the surface tension increases with decreasing bubble diameter. The above expression can also be generalized as

$$\frac{\gamma(r)}{\gamma_0} \approx \frac{1}{1 + 2\delta_T/r} \tag{9.116}$$

where $\delta_T \approx \Gamma/(\rho_d'' - \rho_d')$ is called the Tolman length. It is interpreted as the distance between equimolar surface, where the densities of the liquid phase and the vapor phase are equal, and the surface of the tension. A more accurate expression was given by Tolman (1949).

Typically, the Tolman length is short. Molecular dynamics simulation by Haye and Bruin (1994) found that for the Lennard–Jones potential, $\delta_T/\sigma = 0.2 \pm 0.05$. Since in the Lennard–Jones potential σ is only a few angstroms (3.542 Å for argon), δ_T is very small, so that the effect of radius on surface tension is negligible in most situations. The size dependence of surface tension is of great interest to nucleation theory and has received most attention in this field (Laaksonen et al., 1995). Typically, it is found that the Tolman length is a function of radius and temperature and thus the original theory by Tolman is often modified and revisited (Kalikmanov, 1997; Granasy, 1998).

9.5 Summary of Chapter 9

Because the liquid molecules are closely packed and lack long-range correlations as in crystalline solids, conventional kinetic theory, which is based on the assumption of dilute particles and infrequent interaction among the particles, is not applicable to liquid systems. This difficulty has prevented us from pursuing a treatment of the transport processes in liquid parallel to what we have done for gaseous molecules, electrons, phonons, and photons in previous chapters. This chapter attempts to provide an overview of theoretical tools for studying transport in liquids and key aspects of the interfaces between liquids and their surroundings.

We started with a review of theoretical tools that treat transport in bulk liquids. The radial distribution function provides a useful description of the structure of a liquid and we used it to derive the van der Waals equation of state, which captures the vapor, the liquid, and the liquid–vapor coexisting regions, at least qualitatively. For transport in liquid, one effort is the extension of Boltzmann's kinetic theory for gases to higher

densities. The Enskog equation is an example. This equation includes the effects of the finite size of the molecules and, implicitly, the potential energy exchange. The solutions of the Enskog equation for dense gas, however, are not valid at liquid densities. Einstein started a different line of investigation—Brownian motion in liquids. The major result of his investigation was to relate viscosity to the diffusivity of Brownian particles, which provides a means of estimating the size of Brownian particles (and big molecules). Einstein's work laid the foundation for the later development of linear response theory, which has a much broader impact than just liquid transport. The linear response theory applies equally well to all other transport processes we have discussed in this book so far. We have reserved the linear response theory for the next chapter and, instead, discussed only the Langevin equation. This equation generalizes Brownian motion by splitting the forces acting on a Brownian particle into a resistive term that is proportional to the particle velocity and a random force term that arises from the particle interacting with the surrounding. Although Brownian motion is discussed in the context of particle transport in a liquid, it is a very general phenomenon and has found applications in many different fields. We noted that many studies on transport in fluids are based on linear response theory, which also rely heavily on direct computer simulation; hence the reason that we delay further discussion to the next chapter.

Because potential interaction, with its associated momentum and energy exchange, is an important part of transport in liquid, we next turned our attention to the potentials at the interfaces of the liquid and its surroundings: liquid–solid, liquid–vapor, and liquid–liquid interfaces. These interfacial potentials play a central role in surface chemistry and colloids, and have been extensively studied. However, their impacts on momentum and energy transport processes have yet to be fully explored. The interfacial potentials between surfaces can be constructed from the individual atomic and molecular potentials. These interfacial potentials were discussed under three categories:

1. The van der Waals potential (also called London potential or dispersion potential), which usually leads to an attractive force between surfaces separated by a vacuum. The van der Waals potential can also be repulsive, depending on the medium between the two surfaces, and is characterized by the Hamaker constant.
2. The electric double layer potential, formed as a result of the existence of surface charges and leading to a repulsive force between two surfaces separated by the liquid.
3. The potentials and forces arising from molecular structures near the interface, such as the oscillatory solvation force due to the regular molecular arrangement near a solid surface, the hydration force between hydrophilic surfaces (repulsive) and hydrophobic surfaces (attractive), the steric force due to the overlapping of long molecules (important in polymer systems), and the fluctuation force due to molecular protrusion at mobile surfaces and random thermal fluctuation.

The van der Waals force usually decays as D^{-n} (table 9.1), where D is the separation between surfaces. The electric double layer decays exponentially and its characteristic length is the Debye length, which also depends on ion concentration and thus can be controlled, while the molecular structure forces are typically active within a few molecular diameters of the interface (a few nanometers). From the interfacial potential, one can easily appreciate the concept of surface tension, a key phenomenon for micro- and nanosystems, where the inertial force is normally unimportant and the surface force

dominates as the surface-to-volume ratio increases with decreasing size. The Laplace equation determines the shape of an interface and the Young equation determines the contact angle between a liquid droplet and a solid surface.

In section 9.3, we discussed the effects of size on single-phase liquid transport. There have been many studies on fluid flow and heat transfer in microchannels, but the results have been controversial. Size-dependent viscosity has been reported. Similarly, there exist reports on the deviation of heat transfer in microchannels from the continuum theorem. We caution that these data must be viewed critically. The monumental experimental work of Poiseuille, on fluid flow, which is almost 180 years old, was performed in glass tubes with inner diameter 15 μm and above. Yet his data can be explained by the continuum theory. This fact strongly indicates that discrepancies from more recent experiments in microchannels of comparable diameter, when compared with continuum theory, may not be due to the breakdown of the continuum theory but to the differences of experimental conditions and models used. We also note that, at the other extreme, there have been some studies on liquid transport in nanostructures, mostly based on molecular dynamics simulations. Because the interfacial forces discussed in section 4.2 have an active range from a few nanometers to tens or even hundreds of nanometers, these forces may impact the heat transfer and fluid flow processes in nanostructures. This is a direction that calls for more exploration, perhaps with a combination of simulation and modeling tools. In comparison with pressure-driven flow, however, electrokinetic flow, which is due to the existence of the electric double layer, has been well studied. Two basic motion configurations were discussed: electrophoretic flow due to the motion of the particles, and electro-osmotic flow due to the motion of the ionic solution. Such electrokinetic driven flows are widely used in biotechnology and have also found increasing use in a variety of microfluidic devices.

In the last section, we discussed the size dependence of thermodynamic properties of small particles, such as the phase transition pressure, temperature, and surface tension. The results have been well established but are finding new applications in nanotechnology.

9.6 Nomenclature for Chapter 9

a	constant, eq. (9.6), J m^3
A	Hamaker constant, J
A_s	surface area, m^2
b	volume defined by eq. (9.23), m^3
B	volume per molecule, m^3
c	charge concentration on surface, C m^{-2}
C	coefficient in the atom–atom pair potential, J m^6
D	effective diameter of molecule or spacing between surfaces, m
e	unit charge, C
$\mathscr{E}$	electric field, V m^{-1}
f	one-particle distribution function for molecules, m^{-3}
$f^{(2)}$	two-particle distribution function, m^{-6}
$f^{(N)}$	N-particle distribution function
F	Helmholtz free energy, J; force, N
$\mathbf{F}_D$	drag force, N
g	radial distribution function, eq. (9.1)

h Planck constant, J s
H height, m
J particle number flux, $m^{-2}\ s^{-1}$
k thermal conductivity, $W\ m^{-1}\ K^{-1}$
m mass, kg
n particle or atom number density, m^{-3}
n_r refractive index
N total number of particles
p pressure, $N\ m^{-2}$
$\mathbf{p}$ particle momentum, kg m s^{-1}
q charge, C
Q charge, C
Q_V volumetric flow rate, $m^3\ s^{-1}$
r radius, radial coordinate, or radial separation between particles, m
$\mathbf{r}$ position vector, m
$\mathbf{R}$ random driving force in Brownian motion, N
s entropy per mole, $J\ K^{-1}\ mol^{-1}$
t time, s
T temperature, K
$\mathbf{u}$ Brownian particle velocity or drift velocity, $m\ s^{-1}$
v volume per mole, $m^3\ mol^{-1}$
W work, J
W_{11} cohesion energy between two identical surfaces, $J\ m^{-2}$
W_{12} adhesion energy between two different surfaces, $J\ m^{-2}$
Z canonical partition function, or number of net elementary charge per ion
α electric polarizability, $C^2\ m\ N^{-1}$
β electric dipole moment, C m
γ surface tension, $J\ m^{-2}$ or $N\ m^{-1}$
Γ number density of molecules at the Gibbs surface, m^{-2}
δ Debye length, m
δ_T Tolman length, m
Δh enthalpy or latent heat, $J\ mol^{-1}$
ε Lennard–Jones potential parameter, J
ε_0 dielectric permittivity of vacuum, $C^2\ N^{-1}\ m^{-2}$
ε_r dielectric constant
ζ zeta potential, V
η friction coefficient, s^{-1}
κ_B Boltzmann constant, $J\ K^{-1}$
μ dynamic viscosity, $N\ s\ m^{-2}$
Π quantity defined by eq. (9.21), $kg\ m^{-3}\ s^{-1}$
ρ_d mass density, $kg\ m^{-3}$
ρ_n net charge density, $C\ m^{-3}$
σ Lennard–Jones potential parameter, m
φ volumetric fraction of Brownian particles in a solution
ϕ potential energy between particles, J
Φ total potential energy, J
Ψ electrostatic potential, $J\ C^{-1}$
Ω solid angle, srad
$\hat{\mathbf{\Omega}}$ unit vector connecting two colliding molecules

Subscripts

0 flat surface, far away
d dispersion force
E Enskog model
s surface
x x-component
zp when surface potential is zero

Superscripts

$'$ outside the spherical surface, convex side
$''$ inside the spherical surface, concave side

Symbol

$\langle\rangle$ ensemble or time averaging

9.7 References

Alder, B.J., and Wainwright, T.E., 1967, "Velocity Autocorrelations for Hard Spheres," *Physical Review Letters*, vol. 18, pp. 988–990.

Alder, B.J., Gass, D.M., and Wainwright, T.E., 1970, "Studies in Molecular Dynamics. VIII. The Transport Coefficients for a Hard-Sphere Fluid," *Journal of Chemical Physics*, vol. 53, pp. 3813–3826.

Boon, J.P., and Yip, S., 1980, *Molecular Hydrodynamics*, Dover, New York, p. 26.

Buffat, Ph., and Borel, J.-P., 1976, "Size Effect on the Melting Temperature of Gold Particles," *Physical Review A*, vol. 13, pp. 2287–2298.

Carey, V.P., 1999, *Statistical Thermodynamics and Microscale Thermophysics*, Cambridge University Press, Cambridge, UK, chapter 6.

Chapman, S., and Cowling, T.G., 1953, *The Mathematical Theory of Non-Uniform Gases*, Cambridge University Press, Cambridge, UK.

Choi, S.U.S., Zhang, Z.G., Yu, W., Lockwood, F.E., and Grulke, E.A., 2001, "Anomalous Thermal Conductivity Enhancement in Nanotube Suspensions," *Applied Physics Letters*, vol. 79, pp. 2252–2254.

Defay, R., Prigogine, I., Bellemans, A., and Everett, D.H., 1966, *Surface Tension and Adsorption*, Longmans, London.

Derjaguin, B.V., Churaev, N.V., and Muller, V.M., 1987, *Surface Forces* (translated from the Russian by Kisin, V.I.), New York, Consultants Bureau.

Derjaguin, B.V., and Landau, L., 1941, *Acta Physicochim*, USSR, vol. 14, pp. 633–662.

Einstein, A., 1905, "On the Movement of Small Particles Suspended in a Stationary Liquid Demanded by the Molecular Kinetic Theory of Heat," *Annalen der Physik*, vol. 17, p. 549.

Einstein, A., 1906a, "A New Determination of the Molecular Dimensions," *Annalen der Physik*, vol. 19, pp. 289–306; correction, ibid., vol. 34, pp. 591–592 (1911).

Einstein, A., 1906b, "On the Theory of the Brownian Movement," *Annalen der Physik*, vol. 19, pp. 371–381.

Einstein, A., 1908, "The Elementary Theory of the Brownian Motion," *Zeitschrift für Elektrochemie*, vol. 14, pp. 235–239.

Einstein, A., 1956, *Investigations on the Theory of the Brownian Movement*, ed. R. Furth, Dover, New York.

Enskog, D., 1922, "Kungliga Svenska Vatenskapsakademiens Handlingar," *Ny Föld*, vol. 63, no. 4 (1922). For English translation, see Brush, S.G., 1972, *Kinetic Theory*, vol. 3, Pergamon Press, Oxford.

Ferziger, J.H., and Kaper, H.G., 1972, *Mathematical Theory of Transport Processes in Gases*, North-Holland, Amsterdam, chapter 12.

Freund, J.B., 2002, "Electro-Osmosis in a Nanometer Scale Channel Studied by Molecular Dynamics," *Journal of Chemical Physics*, vol. 116, pp. 2194–2200.

Gibbs, J.W., 1928, *Collected Works*, vol. I, Longmans Green, New York, p. 219.

Goodstein, D.L., 1985, *States of Matter*, Dover, New York, chapter 4.

Granasy, L., 1998, "Semiempirical van der Waals/Cahn–Hillar Theory: Size Dependence of the Tolman Length," *Journal of Chemical Physics*, vol. 109, pp. 9660–9663.

Hamaker, H.C., 1937, "The London–van der Waals Attraction between Spherical Particles," *Physica*, vol. 4, pp. 1058–1072.

Hansen, J.P., and McDonald, I.R., 1986, *Theory of Simple Liquids*, Academic Press, London, chapter 7.

Haye, M.J., and Bruin, C., 1994, "Molecular Dynamics Study of the Curvature Correction to the Surface Tension," *Journal of Chemical Physics*, vol. 100, pp. 556–559.

Heremans, J., Thrush, C.M., Lin, Y.-M., Cronin, S., Zhang, Z., Dresselhaus, M.S., and Mansfield, J.F., 2000, "Bismuth Nanowire Arrays: Synthesis and Galvanomagnetic Properties," *Physical Review B*, vol. 61, pp. 2921–2130.

Hiemenz, P.C., 1986, *Principles of Colloid and Surface Chemistry*, 2nd ed., Marcel Dekker, New York.

Hill, T.L., 1963, *Thermodynamics of Small Systems, Part I*, Benjamin, New York.
Hill, T.L., 1964, *Thermodynamics of Small Systems, Part II*, Benjamin, New York.
Ho, C.-M., and Tai, Y.-C., 1998, "Micro-Electro-Mechanical Systems (MEMS) and Fluid Flow," *Annual Review of Fluid Mechanics*, vol. 30, pp. 579–612.
Israelachvili, J.N., 1992, *Intermolecular and Surface Forces*, 2nd ed., Academic Press, London.
Kalikmanov, V.I., 1997, "Semiphenomenological Theory of the Tolman Length," *Physical Review E*, vol. 55, pp. 3068–3071.
Kittel, C., and Kroemer, H., 1980, *Thermal Physics*, 2nd ed., Freeman and Company, New York.
Kohler, F., 1972, *Liquid State*, Verlag Chemie, Weinheim, chapters 8 and 9.
Koplik, J., and Banavar, J.R., 1995, "Continuum Deductions from Molecular Dynamics," *Annual Review of Fluid Mechanics*, vol. 27, pp. 257–292.
Koplik, J., Banavar, J.R., and Willemsen, J.F., 1989, "Molecular Dynamics of Poiseuille Flow at Solid Surface," *Physics of Fluids A*, vol. 1, pp. 781–794.
Kubo, R., Toda, M., and Hashitsume, N., 1998, *Statistical Physics II*, 2nd ed., Springer, Berlin.
Laaksonen, A., Talanquer, V., and Oxtoby, D.W., 1995, "Nucleation—Measurements, Theory, and Atmospheric Applications," *Annual Review of Physical Chemistry*, vol. 46, pp. 489–524.
Liboff, R.L., 1998, *Kinetic Theory*, Wiley, New York.
Lifshitz, E.M., 1956, "The Theory of Molecular Attractive Force between Solids," *Soviet Physics, JETP* (English Translation), vol. 2, pp. 72–83.
Manchenko, G.P., 2003, *Handbook of Detection of Enzymes on Electrophoretic Gels*, CRC Press, Boca Raton, FL.
Morales, A.M., and Lieber, C.M., 1998, "A Laser Ablation Method for the Synthesis of Crystalline Semiconductor Nanowires," *Science*, vol. 279, pp. 208–211.
Obot, N.T., 2000, "Toward a Better Understanding of Friction and Heat/Mass Transfer in Microchannels—A Literature Review," in *Proceedings of the International Conference on Heat Transfer and Transport Phenomena in Microscale*, ed. G.P. Celata, Begell House, New York, pp. 72–79.
Rice, C.L., and Whitehead, R., 1965, "Electrokinetic Flow in a Narrow Cylindrical Capillary," *Journal of Physical Chemistry*, vol. 69, pp. 4017–4023.
Rice, S.A., and Allnatt, A.R., 1961, "On Kinetic Theory of Dense Fluids. VI. Singlet Distribution Function for Rigid Spheres with an Attractive Potential," *Journal of Chemical Physics*, vol. 34, p. 2144.
Rice, S.A., and Gray, P., 1965, *The Statistical Mechanics of Simple Liquids*, Wiley, New York.
Sengers, J.V., 1965, "Thermal Conductivity and Viscosity of a Moderately Dense Gas," *International Journal of Heat and Mass Transfer*, vol. 8, pp. 1103–1116.
Shockley, W., 1949, "The Theory of p–n Junctions in Semiconductors and p–n Junction Transistors," *Bell System Technical Journal*, vol. 28, pp. 435–489.
Sobhan, C.B., and Garimella, S.V., 2000, "A Comparative Analysis of Studies on Heat Transfer and Fluid Flow in Microchannels," in *Proceedings of the International Conference on Heat Transfer and Transport Phenomena in Microscale*, ed. G.P. Celata, Begell House, New York, pp. 80–92.
Sutera, S.P., and Skalak, R., 1993, "The History of Poiseuille's Law," *Annual Review of Fluid Mechanics*, vol. 25, pp. 1–19.
Thompson, P.A., and Robbins, M.O., 1990, "Shear Flow Near Solids: Epitaxial Order and Flow Boundary Conditions," *Physical Review A*, vol. 41, pp. 6830–6837.
Thompson, P.A., and Troian, S.M., 1997, "A General Boundary Condition for Liquid Flow at Solid Surfaces," *Nature*, vol. 389, pp. 360–362.
Tolman, R.C., 1949, "The Effect of Droplet Size on Surface Tension," *Journal of Chemical Physics*, vol. 17, pp. 333–337.
Velarde, M.G., 1974, "On the Enskog Hard-Sphere Kinetic Equation and the Transport Phenomena of Dense Simple Gases," in *Transport Phenomena*, ed. G. Kirczenow and J. Marro, Springer-Verlag, Berlin, pp. 289–336.

Verwey, E.J.W., and Overbeek, J. Th. G., 1948, *Theory of Stability of Lyophobic Colloids*, Elsevier, Amsterdam.
Wayner, P.C., Jr, 1998, "Interfacial Forces and Phase Change in Thin Liquid Films," in *Microscale Energy Transport*, ed. C.L. Tien, A. Majumdar, and F.M. Gerner, Taylor & Francis, Washington, DC.

9.8 Exercises

9.1 *van der Waals equation of states—critical point and the corresponding states.* The critical point of a liquid is where the D and E points in figure 9.2 coincide with each other. This is an inflection point (point where both the first-order and the second-order derivatives are zero) on the constant T curve in a p–V diagram.

(a) Start from the van der Waals equation, and demonstrate the critical temperature T_c and pressure p_c

$$T_c = \frac{8a}{27B\kappa_B} \text{ and } P_c = \frac{a}{27B^2}$$

(b) Show that the van der Waals equation can be written as

$$p_r = \frac{8T_r}{3v_r - 1} - \frac{3}{v_r^2}$$

where $p_r = p/p_c$, $T_r = T/T_c$, and $v_r = V/V_c$. Thus, in this normalized form, the equation of states is independent of the actual fluids. This is called the law of corresponding states.

9.2 *Saturation pressure.* The saturation pressure, line A and B in figure 9.2 can be found by requiring that the chemical potentials of the liquid and the vapor phases are equal to each other. Derive a relation between the saturation pressure and temperature for a van der Waals liquid.

9.3 *Enskog equation.* Argon gas at low density and 300 K has a thermal conductivity of 0.018 $\mathrm{W\,m^{-1}\,K^{-1}}$. Estimate its thermal conductivity as a function of density at higher density. In what range do you expect this estimation to be valid?

9.4 *Einstein relation.* The viscosity of water at 300 K is 4×10^{-4} $\mathrm{N\,s\,m^{-2}}$ and the diffusivity of monodisperse Brownian particles in water is 1.1×10^{-11} $\mathrm{m^2\,s^{-1}}$. Estimate the diameter of the particle.

9.5 *Viscosity of nanofluids.*

(a) The viscosity of water is 4×10^{-4} $\mathrm{N\,s\,m^{-2}}$. Nanoparticles are seeded into water with a volume concentration of 5%. What is the viscosity of the nanoparticle-loaded fluid according to the Einstein theory?

(b) The Einstein theory is based on the assumption of dilute particles such that interparticle interactions can be neglected. Estimate the interparticle distance for a 5% volume loading as a function of the nanoparticle diameter, assuming that nanoparticles are monodisperse.

9.6 *Van der Waals potential between two nanowires.* Carbon nanotubes and nanowires can be grown into aligned and closely spaced dense arrays [see figure 1.4(c)]. Estimate the van der Waals potential and the attractive force per unit length between two parallel silicon nanowires of equal diameter (10 nm) with a center-to-center spacing of 20 nm. Assume $C = 5 \times 10^{-78}$ $\mathrm{J\,m^6}$. The silicon lattice constant is 5.2 Å.

9.7 *Debye length.* Estimate the Debye length in water containing 0.01 mole of NaCl. The dielectric constant of water is 78.54.

9.8 *Liquid helium and disjoining pressure.* It is known that if liquid helium is placed in a beaker, it rapidly climbs up the walls and down the other side, and eventually leaves the container. This is caused by a negative Hamaker constant between the helium vapor and the container wall.

(a) Show that the liquid helium film varies as a function of its thickness,

$$D = \left(-\frac{A}{6\pi\rho g H}\right)^{1/3}$$

(b) The Hamaker constant between helium vapor and the container, made of CaF_2, is -0.59×10^{-20} J. Estimate the liquid helium film height at a thickness of $D = 2$ nm. The density of liquid helium is 125 kg m^{-3}.

9.9 *Capillary rise of liquid in a tube.* In a small tube inserted into a liquid bath, the liquid rises above the height of the bath surface due to the surface tension if the contact angle is less than 90° (figure P9.9). Show that the height of the liquid column is

$$H = \frac{2\sigma \cos\theta}{(\rho_l - \rho_v)\, g r_i}$$

where ρ_l and ρ_v are the density of the liquid and its vapor and r_i is the inner radius of the capillary tube. For glass tubes with $r_i = 10$ μm, 100 μm, and 1 mm, estimate the heights of water inside the tube ($\gamma = 72.8$ mN m^{-1})

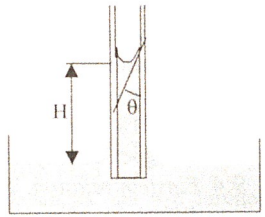

Figure P9.9 Figure for exercise 9.9.

9.10 *Electrokinetic flow.* Consider fully developed electro-osmotic flow between two parallel plates, assuming that the Debye thickness is much smaller than the separation of the two plates. Use the Hückel–Debye approximation to find the electric double layer potential distribution,

(a) Develop an expression for the velocity distribution within the electric double layer.

(b) Assuming that a constant heat flux is applied to the fluid on both surfaces and the thermal profile is fully developed, derive an expression for the Nusselt number.

9.11 *Effects of radius on water droplet surface tension and saturation vapor pressure.* For water, taking 9.6 $Å^2$ as the surface area occupied by a water molecule on the surface of tension, half of the monolayer concentration is $\Gamma = 0.9 \times 10^{-9}$ mol cm^{-2}. The liquid phase density is $\rho'' = 5.55 \times 10^{-2}$ mol cm^{-3}. Calculate the surface tension and the saturation vapor pressure of water droplets as a function of the diameter in the range of $r = 10^{-9}$–10^{-6} m.

9.12 *Effects of radius on water vapor bubble surface tension and saturation vapor pressure.* Using the same data as in exercise 9.11, calculate the surface tension and the saturation vapor pressure of a water bubble inside water as a function of its diameter in the range of $r = 10^{-9}$–10^{-6} m.

9.13 *Melting temperature of Au nanoparticles.* The surface tension between liquid and solid gold is 0.27 N m^{-1}, and its latent heat is 6.27×10^4 J kg^{-1}. Estimate the melting temperature of gold nanoparticles as a function of their radius. The melting point of bulk gold is 1064.43°C.

9.14 *Bismuth condensation into anodized alumina template.* Consider the condensation of bismuth vapor onto an anodized alumina template with cylindrical channels. The channel diameter is between 5 and 20 nm. Comment on the filling process of superheated bismuth vapor into the channel. The surface tension of bismuth is 378×10^{-3} N m^{-1} at melting point 271°C.